Review article **Open Access**

Yong-Chun Liu*, Bei-Bei Li* and Yun-Feng Xiao*

Electromagnetically induced transparency in optical microcavities

DOI 10.1515/nanoph-2016-0168
Received October 10, 2016; revised January 5, 2017; accepted January 10, 2017

Abstract: Electromagnetically induced transparency (EIT) is a quantum interference effect arising from different transition pathways of optical fields. Within the transparency window, both absorption and dispersion properties strongly change, which results in extensive applications such as slow light and optical storage. Due to the ultra-high quality factors, massive production on a chip and convenient all-optical control, optical microcavities provide an ideal platform for realizing EIT. Here we review the principle and recent development of EIT in optical microcavities. We focus on the following three situations. First, for a coupled-cavity system, all-optical EIT appears when the optical modes in different cavities couple to each other. Second, in a single microcavity, all-optical EIT is created when interference happens between two optical modes. Moreover, the mechanical oscillation of the microcavity leads to optomechanically induced transparency. Then the applications of EIT effect in microcavity systems are discussed, including light delay and storage, sensing, and field enhancement. A summary is then given in the final part of the paper.

Keywords: electromagnetically induced transparency; microcavity; coupled cavities; optomechanics; interference.

***Corresponding authors: Yong-Chun Liu,** Qian Xuesen Laboratory of Space Technology, China Academy of Space Technology, Beijing 100094, P.R. China; and Department of Physics, Tsinghua University, Beijing 100084, P.R. China, e-mail: ycliu@tsinghua.edu.cn; **Bei-Bei Li,** Qian Xuesen Laboratory of Space Technology, China Academy of Space Technology, Beijing 100094, P.R. China, e-mail: libeibei0036@gmail.com; and **Yun-Feng Xiao,** State Key Laboratory for Mesoscopic Physics and School of Physics, Peking University, Beijing 100871, P.R. China; and Collaborative Innovation Center of Quantum Matter, Beijing 100871, P.R. China, e-mail: yfxiao@pku.edu.cn

1 Introduction and physical basis

Electromagnetically induced transparency (EIT) is a phenomenon in which an electromagnetic field controls the optical response of the material. It is first observed in gas-phase atomic medium [1, 2], which predicts that the absorption of the three-level atomic ensembles is canceled in the presence of an auxiliary electromagnetic field. The phenomenon arises from the quantum interference effect, where the transition amplitudes of different pathways destructively interfere. The EIT effect has led to broad applications in optical and quantum information processing. In particular, the abnormal dispersion occurs with the opening of the transparency window, resulting in a dramatic reduction of the light group velocity, i.e. slow light [3, 4]. It even enables the complete stop of the propagating optical pulse, meaning that the light pulse can be stored in the atomic ensembles [5, 6]. The slow and stopped light is important in optical networks [7] for implementing optical buffer, and it is also applicable for quantum networks [8] in building quantum memory [9, 10]. Some reviews on EIT in atomic systems can be found in Refs. [11–20].

The basic principle of EIT is illustrated in Figure 1. The energy levels of a lambda-type three-level atom is plotted in Figure 1A, where state $|1\rangle$ is the ground state, state $|2\rangle$ is a metastable state, and state $|3\rangle$ is an excited state. Correspondingly, the radiative decay rate of state $|3\rangle$ is much larger than that of state $|2\rangle$ ($\Gamma_3 \gg \Gamma_2$). The transitions $|1\rangle$–$|3\rangle$ and $|2\rangle$–$|3\rangle$ are dipole-allowed transitions, while $|1\rangle$–$|2\rangle$ is dipole-forbidden transition. The control field couples state $|2\rangle$ and state $|3\rangle$, and the probe field couples state $|1\rangle$ and state $|3\rangle$. Without the control field, the probe field is absorbed by the atom via the $|1\rangle$–$|3\rangle$ transition when on resonance, and thus the atomic medium is opaque to the probe field. In the presence of the strong control field, quantum interference occurs, and the atomic medium becomes transparent to the probe field.

To understand the quantum interference in EIT, there are two alternative and equivalent pictures: bare state picture and dressed state picture. In the bare state picture, to excite state $|3\rangle$, there are two different excitation pathways: directly via the $|1\rangle$–$|3\rangle$ pathway or indirectly via the

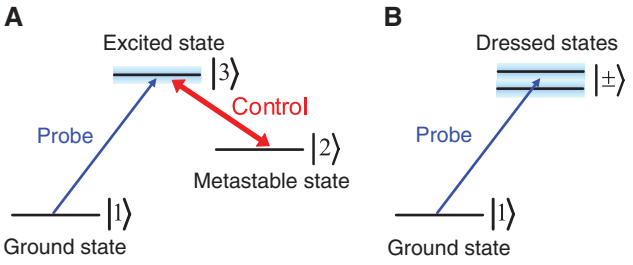

Figure 1: Energy levels in atomic EIT systems.
(A) Bare-state picture of the lambda-type three-level system.
(B) Dressed-state picture of the EIT system. See text for details.

$|1\rangle-|3\rangle-|2\rangle-|3\rangle$ pathway. As the control field is more intense than the probe field, and the decay rate of state $|2\rangle$ is small, this indirect pathway has a probability amplitude that is of comparable magnitude to the direct pathway. For resonant fields, the coupling from $|3\rangle$ to $|2\rangle$ leads to $\pi/2$ phase shift, and the coupling from $|2\rangle$ to $|3\rangle$ leads to another $\pi/2$ phase shift. Therefore, the probability amplitude of the indirect excitation pathway has a π phase shift compared with the direct excitation pathway, resulting in destructive interference, and thus the transitions are canceled. Note that the field detuning will modify the phase shift, and in this case, the phase difference for the two excitation pathway is not exactly π, which leads to Fano-type lineshape [21] for the transmission of the probe field.

In the dressed state picture, the strong control field couples state $|2\rangle$ and state $|3\rangle$, leading to two dressed states (Figure 1B), which effectively decays to the same continuum [2, 22, 23]. When the probe field is resonant to the $|1\rangle-|3\rangle$ transition, the contributions from the two dressed states are equal but with an opposite sign, leading to the cancelation of the response, which is a Fano-like interference of the decay channels.

In the following, some formulas are presented to describe the EIT/Fano effect. Using the quantum jump approach [24, 25], the effective system Hamiltonian is given by

$$H_{\text{eff}}=\left(-\Delta_1-i\frac{\Gamma_3}{2}\right)\sigma_{33}+\left(-\Delta_2-i\frac{\Gamma_2}{2}\right)\sigma_{22}+(\Omega_c\sigma_{23}+\Omega_p\sigma_{13}+\text{H.c.}), \tag{1}$$

where $\sigma_{jk}=|j\rangle\langle k|$ is the atomic projection operator (j, $k=1$, 2, 3), $\Delta_1=\omega_p-\omega_{13}$ is the probe field detuning with respect to $|1\rangle-|3\rangle$ transition, and $\Delta_2=\omega_c-\omega_{23}$ is the control field detunings with respect to $|2\rangle-|3\rangle$ transition, Ω_c and Ω_p represent the control and probe field strengths. In the Shrödinger picture, the equations of motion for the probability amplitude of the atom at state $|k\rangle$ ($k=1$, 2, 3) are given by

$$\begin{aligned}\dot{c}_1&=-i\Omega_p^*c_3,\\ \dot{c}_2&=\left(i\Delta_2-\frac{\Gamma_2}{2}\right)c_2-i\Omega_c^*c_3,\\ \dot{c}_3&=\left(i\Delta_1-\frac{\Gamma_3}{2}\right)c_3-i\Omega_c c_2-i\Omega_p c_1.\end{aligned} \tag{2}$$

From the above equations, we can directly find that the variation of c_3 has two source terms: one term is proportional to $\Omega_c c_2$ and the other term is proportional to $\Omega_p c_1$. This indicates the interference between two excitation pathways. The probe field is assumed to be weak ($\Omega_p\ll\Omega_c$), and thus $c_1\simeq 1$, then the steady-state solution is given by

$$c_3=\frac{i\Omega_p}{i\Delta_1-\frac{\Gamma_3}{2}+\frac{|\Omega_c|^2}{i\Delta_2-\frac{\Gamma_2}{2}}}. \tag{3}$$

Without the control field ($\Omega_c=0$), for the resonant case ($\Delta_1=0$), the probability of the atom at state $|3\rangle$ is given by $|c_3|^2=4|\Omega_p|^2/\Gamma_3^2$. However, in the presence of the control field, for the two-photon resonant case ($\Delta_1=\Delta_2=0$), the probability is changed to $4|\Omega_p|^2/\left(\Gamma_3+\frac{4|\Omega_c|^2}{\Gamma_2}\right)^2$. It shows that the interference effectively reduces the probability of the atom at state $|3\rangle$, which indicates that light is less absorbed by the atoms, corresponding to a transparency window in the transmission spectrum.

The EIT/Fano effect discussed above requires gas-phase three-level atoms, which greatly limits its applications. One recent fascinating development is the realization of EIT/Fano effect in solid-state optical microcavity systems [26–58] and nanoscale plasmonic and metamaterial structures [59–67]. These optical systems possess resonant modes, which play the roles of the atomic energy levels. Most importantly, the optical microcavity systems allow for on-chip integration and room-temperature operation, and the resonant modes can be tuned to almost any wavelength range. With the rapid development of the micro/nano fabrication techniques, optical microcavities with ultrahigh quality factors (Q) and small mode volumes are widely studied [68–70], which have sought applications ranging from fundamental physics to applications, such as cavity quantum electrodynamics [71, 72], nonlinear optics [73], low-threshold microlasing [74], and biosensing [75–82].

In the microcavity system, the EIT/Fano effect involves two optical modes. The field of the first (second) cavity mode corresponds to the probability amplitude of

the atom at the excited (metastable) state. The coupling between the two cavity modes corresponds to the control field, and the input of the first cavity mode corresponds to the probe field. The effective Hamiltonian of the system is given by

$$H_{\text{eff}} = \left(-\Delta_1 - i\frac{\kappa_1}{2}\right)a_1^\dagger a_1 + \left(-\Delta_2 - i\frac{\kappa_2}{2}\right)a_2^\dagger a_2 + J(a_1^\dagger a_2 + a_2^\dagger a_1) + (\Omega_p a_1^\dagger + \text{H.c.}), \tag{4}$$

where a_1 and a_2 are the field operators of the two cavity modes, J is the coupling strength between the two cavity modes, κ_1 and κ_2 are the decay rates of the two cavity modes, and $\Delta_1 = \omega_p - \omega_1$ and $\Delta_2 = \omega_p - \omega_2$ are the detunings of the probe field with respect to the first and second cavity modes, respectively. The equations of motion for the field of the cavity modes are given by

$$\dot{a}_1 = \left(i\Delta_1 - \frac{\kappa_1}{2}\right)a_1 - iJa_2 - i\Omega_p,$$
$$\dot{a}_2 = \left(i\Delta_2 - \frac{\kappa_2}{2}\right)a_2 - iJa_1. \tag{5}$$

Then the steady-state solution is given by

$$a_1 = \frac{i\Omega_p}{i\Delta_1 - \frac{\kappa_1}{2} + \frac{J^2}{i\Delta_2 - \frac{\kappa_2}{2}}}. \tag{6}$$

From the above derivations, we find that EIT in optical microcavities exactly matches that in atomic systems. By comparing Eqs. (3) and (6), we obtain the following direct correspondence: $\Omega_c \leftrightarrow J$, $\Gamma_3 \leftrightarrow \kappa_1$, and $\Gamma_2 \leftrightarrow \kappa_2$. In optical cavity systems, another natural approach to understand EIT is the bright and dark mode description. The first cavity mode corresponds to the bright mode, which can couple to the external field; the second cavity mode plays the role of a dark mode, which only couples to the first cavity mode but does not couple to the external field. This description is in equivalence to the three-level explanation.

Using the input-output relation, the transmission can be obtained as

$$T = \left| \frac{-i\Delta_1 + \frac{J^2}{-i\Delta_2 + \frac{\kappa_2}{2}}}{-i\Delta_1 + \frac{\kappa_1}{2} + \frac{J^2}{-i\Delta_2 + \frac{\kappa_2}{2}}} \right|^2, \tag{7}$$

where we have assumed critical coupling for $J = 0$ case. The EIT transparency window can be further described by a Lorentzian lineshape written as

$$T_{\text{EIT}} \simeq \left| \frac{\frac{C\kappa_2}{2}}{-i\Delta_2 + \frac{(C+1)\kappa_2}{2}} \right|^2, \tag{8}$$

where $C = 4J^2/(\kappa_1\kappa_2)$ is the cooperativity parameter. From Eq. (8), we can obtain the full width at half maximum (FWHM) of the transparency window $\Gamma_{\text{EIT}} = (C+1)\kappa_2$, and the peak value of transmission $T_{\max} = C^2/(C+1)^2$. The group delay $\tau = -d\phi/d\omega$ at the transparency window is given by $\tau_0 = 2/[(C+1)\kappa_2] = 2/\Gamma_{\text{EIT}}$. Therefore, the cooperativity C is an important parameter, which characterizes the properties of EIT window. To observe EIT phenomenon, it requires $C \gg 1$.

In Figure 2, typical intracavity field intensity and phase shift are plotted. The two cavity modes are assumed to have the same resonance frequency but different decay rates ($\kappa_2 = 0.01\kappa_1$). Without the coupling between the two cavity modes (blue dashed curves), the field intensity has a Lorentzian lineshape, and the phase shift changes slowly when the probe laser frequency scans through the resonance. With the coupling between the two cavity modes (red solid curves), EIT effect occurs, which is manifested by a sharp window in the Lorentzian lineshape of the field intensity and an abrupt change of the phase shift near the EIT window. One may see that this EIT lineshape is somewhat similar to the Autler-Townes splitting phenomenon with two spitted resonances. However, EIT and Autler-Townes splitting phenomena are essentially different, with the differences extensively discussed recently [83, 84].

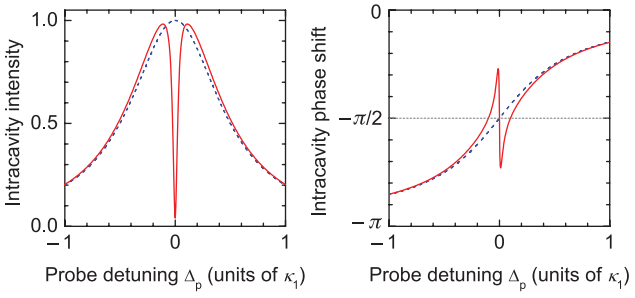

Figure 2: Typical intensity (normalized) and phase shift of the intracavity field.The red solid (blue dashed) curves correspond to the case in the presence (absence) of the control field. The two cavity modes possess the same resonance frequency ($\Delta_p = \Delta_1 = \Delta_2$), $\kappa_2 = 0.01\kappa_1$ and $J = 0.1\kappa_1$.

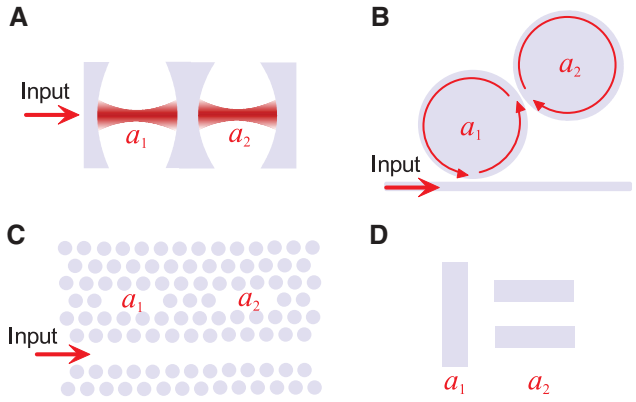

Figure 3: Coupled-cavity systems for the realization of EIT/Fano effect.
(A) Fabry-Perot cavity system. (B) Whispering-gallery mode cavity system. (C) Photonic crystal cavity system. (D) Plasmonic cavity system.

To realize such EIT/Fano effect, the most direct method is to use coupled cavities. Typical coupled-cavity systems are plotted in Figure 3, including Fabry-Pérot (FP) cavity system, whispering-gallery mode (WGM) cavity system, photonic crystal cavity system, and plasmonic cavity system. An alternative approach is employing one single cavity, which simultaneously supports two optical modes with intermode coupling. Moreover, by making use of the mechanical motional degree of freedom, EIT/Fano effect can be realized in optomechanical systems with an optical mode coupled to a mechanical mode. The following parts of the review are organized as follows. In Section 2, we provide an introduction on all-optical EIT in coupled microcavities; in Section 3, the topic of all-optical EIT in a single microcavity is reviewed; in Section 4, we discuss recent progresses on optomechanically induced transparency. In Section 5, the potential applications are discussed. Finally, a summary is presented in Section 6.

2 All-optical EIT in coupled microcavities

In coupled cavities, the coupling between modes from different cavities produces EIT/Fano resonance. In this section, we will review EIT/Fano resonance in several different cases, including FP cavity coupled with a WGM cavity, Mach-Zehnder interferometer (MZI) coupled with WGM cavity, directly coupled WGM cavity system, indirectly coupled WGM cavity system via two parallel waveguides, and indirectly coupled WGM cavity system via one single waveguide.

The earliest study on EIT/Fano resonance in microcavity system was introducing an FP cavity in the waveguide, which is coupled to the WGM cavity. In 2002, Fan proposed to use two partially reflected elements in the coupling waveguide as the FP cavity to generate the coupling between FP and WGM cavities to produce Fano resonance [26], as shown in Figure 4A and B. Later in 2003, Chao and Guo [27] fabricated a polystyrene microcavity using nanoimprint method and made an FP cavity by introducing two offsets in the polystyrene waveguide. They observed the Fano resonance induced by the coupling between the FP cavity and the WGM cavity and realized Fano resonance enhanced biosensing. In 2006, Liang et al. also observed EIT resonance in an FP-WGM coupled cavities by introducing a Bragg grating in the coupling fiber [28], as shown in Figure 4C and D. Lu et al. proposed an MZI structure with one arm coupled with a microcavity resonator to produce tunable Fano resonance and studied the bistability in this structure. And then Zhou et al. demonstrated the Fano resonance engineered add-drop filter in an MZI with one arm coupled with a silicon ring resonator and the other arm driven by a bias voltage [30], as shown in Figure 4E and F.

In two or more WGM microcavities, modes from different cavities can also directly couple with each other through their evanescent field and produce EIT/Fano resonance. In 2004, Smith et al. theoretically studied the EIT resonance in a multiple directly coupled cavity system [31], as shown in Figure 5A. Then in 2005, Naweed et al. observed EIT resonance in two directly coupled silica microspheres [34], as shown in Figure 5B. In 2007, Totsuka et al. experimentally studied the slow light effect when EIT resonance appears in two directly coupled microsphere system (Figure 5C) [36].

In directly coupled cavity case, the distance between cavities needs to be very precisely controlled, while different cavities can also be indirectly coupled through the coupling waveguide, without the requirement of controlling the distance between cavities. In 2006, Xu et al. studied the EIT resonance in two silicon ring resonators indirectly coupled through two parallel waveguides [37] (Figure 6A), and in 2007, they investigated the slow light effect in this structure [38]. In 2007, Xiao et al. further studied the EIT effect in multiple-cavity system also indirectly coupled through two parallel waveguides [43]. Their result showed that N indirectly coupled microcavities produce $N-1$ EIT frequency transparency windows in the transmission spectrum, as shown in Figure 6B.

In the abovementioned indirectly coupled cavity systems, two parallel waveguides are required to induce the coupling between cavities by making the optical field

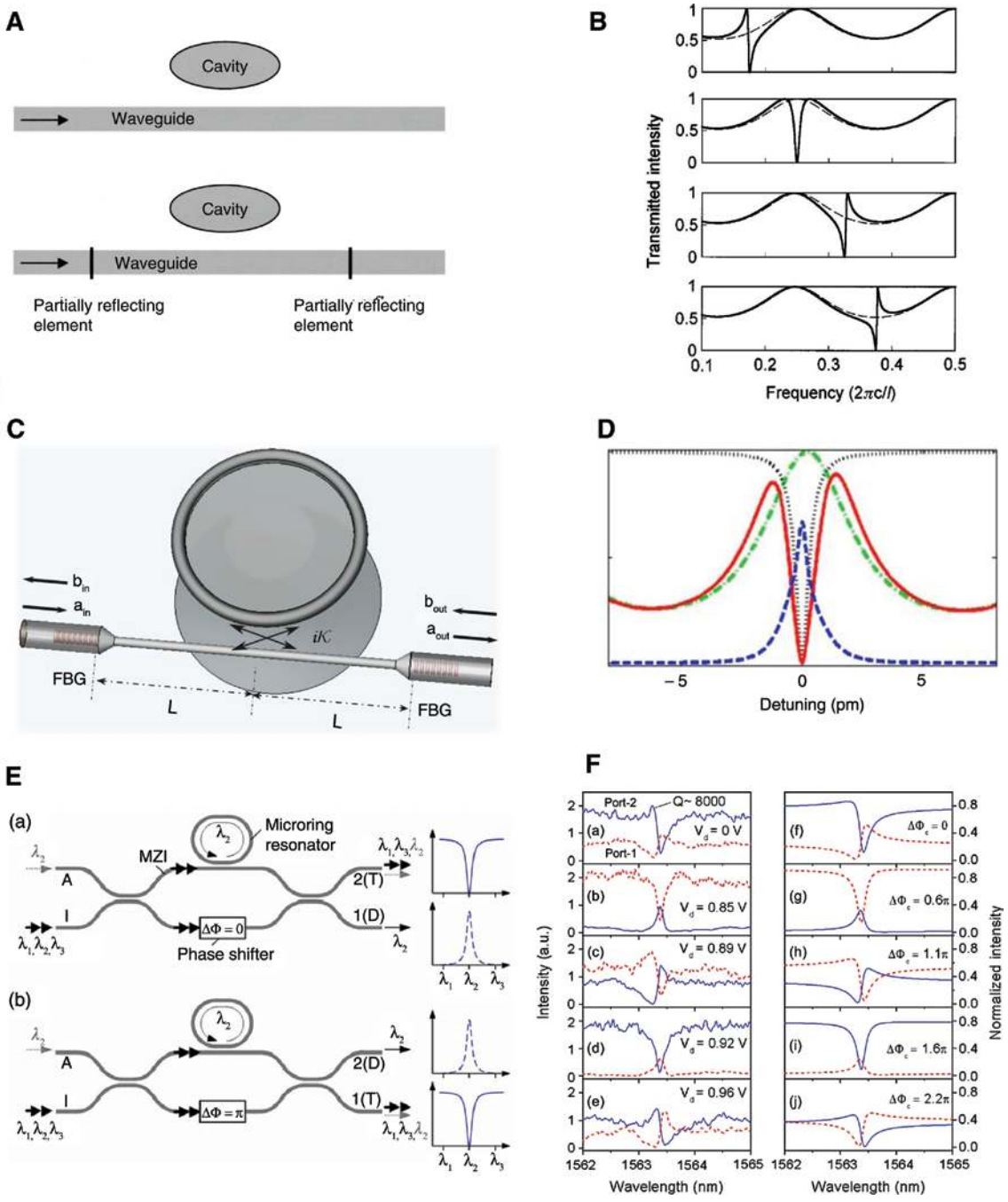

Figure 4: Fano/EIT resonance in a FP-WGM coupled cavities system (A and B), fiber Brag grating coupled with a WGM cavity system (C and D), and a Mach-Zehnder interferometer system with one arm coupled with a ring resonator (E and F).
Figures reproduced with permission from (A and B) Ref. [26], Copyright 2002 AIP; (C and D) Ref. [28], Copyright 2007 OSA. (E and F) Ref. [30], Copyright 2007 OSA.

reflecting back and forth along the waveguides between cavities. If the cavities can couple to the waveguide to both directions, e.g. for standing wave cavities, then one waveguide can also induce the indirect coupling between different cavities. In the view of experimental fabrication, this will greatly decrease the complexity. In 2008, Xiao et al. [39, 40] used transfer matrix method to study the physical origin of Fano resonance produced by two cavities indirectly coupled through one side-coupled waveguide. They further discussed the capability of using the Fano resonance to enhance the sensitivity of biosensing, showing that the sensitivity

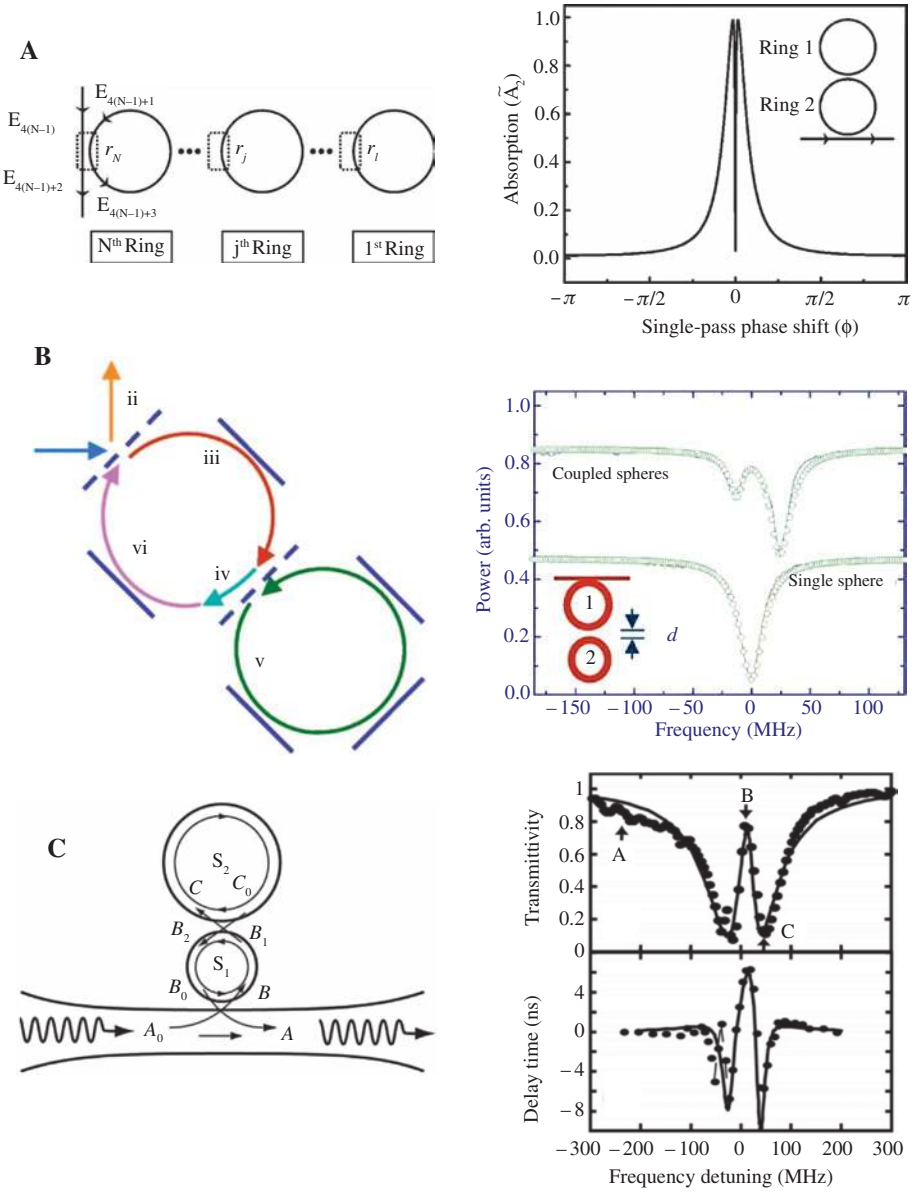

Figure 5: EIT/Fano resonance in directly coupled cavity system.
Figures reproduced with permission from (A) Ref. [31], Copyright 2004 APS; (B) Ref. [34], Copyright 2006 APS; (C) Ref. [36], Copyright 2007 APS.

can be enhanced by 12 times benefiting from the sharp slope in the transmission spectrum [40] (Figure 7A). In 2010, Xiao et al. studied the same coupled cavity system using coupled mode theory and explained the physics of the Fano resonance more intuitively. They also proposed to use the intensity change of the absorption dip of the Fano resonance as the sensing signal [41] (Figure 7B). It showed that the transmission or reflection spectra exhibit periodic change when the distance between the two cavities changes, as the accumulated phase of the light propagating in between the two cavities changes periodically. To realize the indirectly coupled cavity system via a single waveguide, Li et al. demonstrated a free WGM microdisk coupled with a microtoroid through a fiber taper [42]. In order for this, they etched the silicon pedestal of a microdisk to be smaller than 5 μm, then used a three-dimensional nano-stage to control the microdisk to approach a fiber taper. Then the disk can be separated from its silicon pedestal and stick to the fiber taper through Van der Waals force, as shown in Figure 7C. Then another toroid cavity can be directly coupled to the same fiber taper. In this system, the position of the microdisk is fixed and that of the toroid can be controlled by the nano-stage. As a result, the distance L between the two cavities can be adjusted, which will engineer the coupling strength between the two cavities.

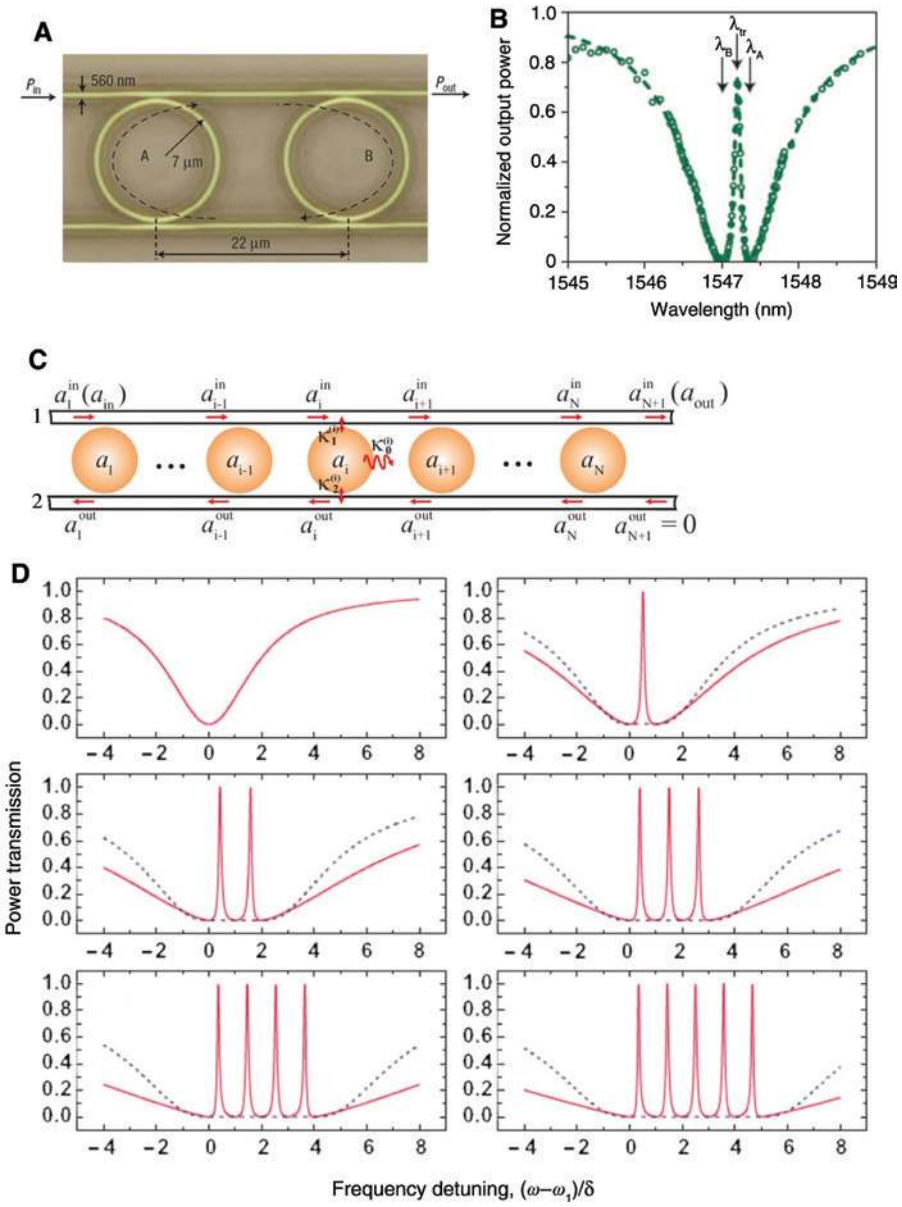

Figure 6: EIT resonance in indirectly coupled cavity system via two parallel waveguides.
Figures reproduced with permission from (A and B) Ref. [37], Copyright 2006 APS; (C and D) Ref. [43], Copyright 2007 APS.

As shown in Figure 7D, the transmission spectrum of the microdisk/microtoroid coupling system changes periodically between a Lorentz dip and an asymmetric Fano lineshape, when the distance L is adjusted.

3 All-optical EIT in a single microcavity

In a single microcavity, different optical resonance modes are originally orthogonal and do not couple with each other. However, indirect coupling can be induced by the coupling waveguide, thus producing EIT or Fano resonance through the interference between two different pathways associated with the two optical modes. And in the perspective of experiment, realization of EIT/Fano resonance in a single microcavity greatly decreases the experimental complexity compared with that in coupled cavity systems. In this section, we first talk about some experimental results of EIT/Fano resonance in a single microcavity and then introduce a theoretical model to explain the physics of the EIT/Fano resonance in a single microcavity.

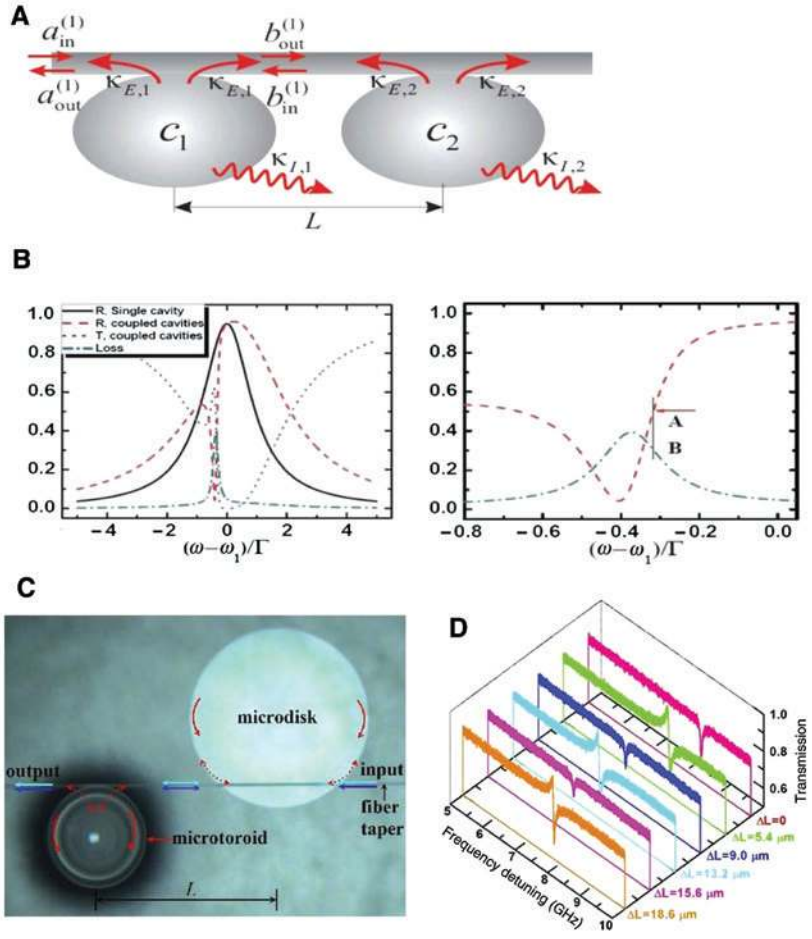

Figure 7: Fano resonance in indirectly coupled cavity system via a single side-coupled waveguide.
Figures reproduced with permission from (A) Ref. [40], Copyright 2008 OSA; (B) Ref. [41], Copyright 2010 APS. (C) Ref. [42], Copyright 2012 AIP.

3.1 Experimental realization of EIT in a single microcavity

Realization of EIT/Fano resonance in a single microcavity requires two spectrally overlapped optical cavity modes to couple to each other. The first experimental demonstration of EIT resonance in a single microcavity was done in a polydimethylsiloxane (PDMS)-coated silica microtoroid by Xiao et al. [44]. They fabricated the microtoroid using the standard photolithography, XeF_2 etching, and CO_2 laser reflow process, as was done in Ref. [77]. Then they coated the microtoroid with a layer of PDMS using the method introduced in Ref. [85]. The PDMS layer is used to thermally tune two different optical modes on-resonance, as WGMs in such a coated microtoroid have distinct thermal response, red-shifting or blue-shifting with temperature increasing, depending on the ratio of light energy distributing in the silica core and the PDMS cladding layers. As a result, two WGMs in a single microcavity, which are originally separated in the spectrum, can experience different frequency shifts with the same temperature variation and be tuned on resonance. As shown in Figure 8A, when the two modes are separated, the transmission spectrum exhibits two separated Lorentzian dips, and when they are spectrally overlapped by temperature tuning, a sharp transparency window appears at the frequency of the high-Q resonance. Dong et al. also observed similar EIT resonance in a pure silica spherical cavity without coating [45]. In microspheres, more optical modes are supported and it is easier to find two spectrally overlapped modes. In this work, they changed the frequency detuning between the two modes through changing the coupling strength between the cavity and the fiber taper by adjusting the distance between them. This is because changing the coupling strength can alter the effective refractive indices of the two modes differently. Figure 8B shows the transmission spectra with the transparency window appearing at different frequencies with different taper-cavity distance.

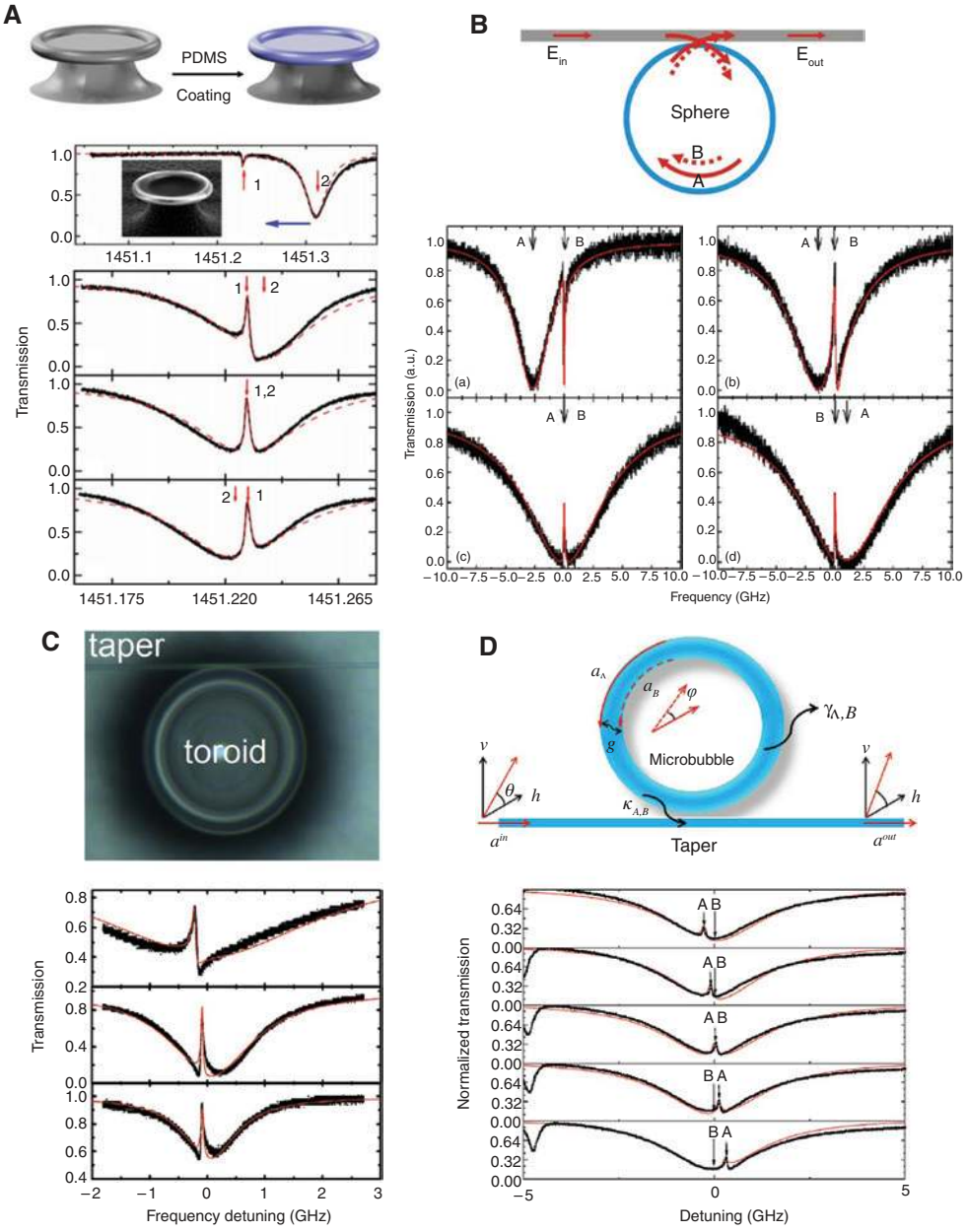

Figure 8: EIT resonance in different single microcavity systems: (A) a PDMS-coated silica toroidal microcavity, (B) a single microsphere cavity, (C) a single microtoroid cavity, and (D) a single microbubble cavity.
All the black curves are the experimental results, and the red ones are the corresponding theoretical results. Figures reproduced with permission from (A) Ref. [44], Copyright 2009 AIP, (B) Ref. [45], Copyright 2009 IOP, (C) Ref. [46], Copyright 2011 AIP, and (D) Ref. [47], Copyright 2015 OSA.

Li et al. [46] then experimentally observed both EIT and Fano resonance lineshapes in a pure silica toroidal cavity when a high-Q and a low-Q optical modes are simultaneously excited through a fiber taper. They found that the EIT and Fano lineshapes can convert to each other when changing the coupling strength between the fiber taper and the cavity by adjusting the taper-cavity gap distance, as shown in Figure 8C. When both the high-Q and low-Q modes are over-coupled, the transmission spectrum exhibits a Fano lineshape, and when the high-Q mode is over-coupled and the low-Q mode is under-coupled or critical-coupled, the transmission spectrum shows an EIT lineshape. Very recently, EIT resonance was also observed in a microbubble resonator coupled with a fiber taper by pressure tuning to make the two optical modes overlap [47], with the result shown in Figure 8D.

Another type of Fano resonance in a single microcavity was also realized through a single cavity mode coupled with a multi-mode waveguide [48]. In this work, multimode waves propagating in a 2.3-μm-diameter taper were coupled with a single WGM in a 220-μm sphere and their coherent interaction resulted in Fano resonance (Figure 9A). The asymmetric lineshape of the transmission spectrum changed periodically when scanning the coupling position along the taper, as shown in Figure 9B. The observed 24-μm period was due to the modal dispersion in the tapered fiber.

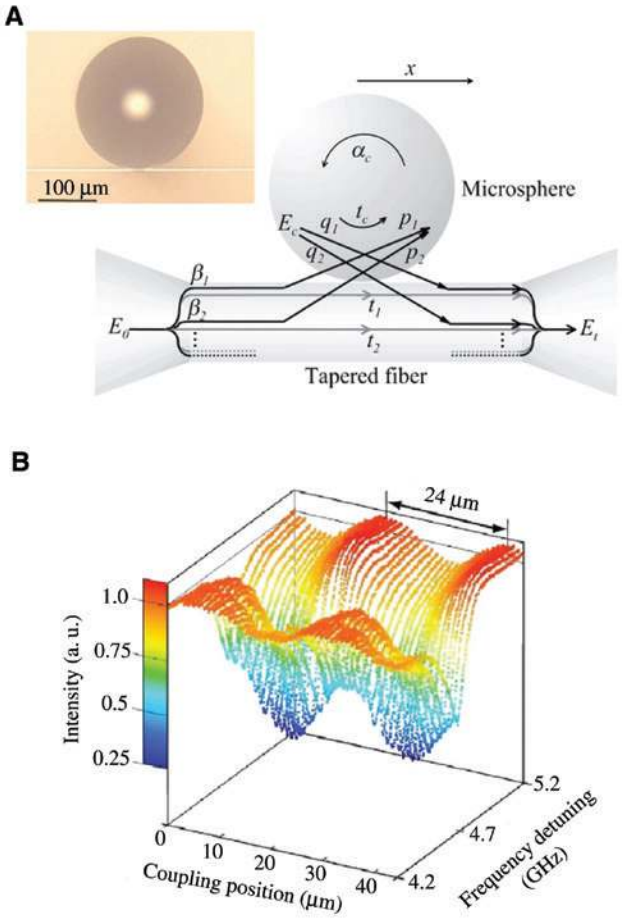

Figure 9: (A) A sketch of a multimode tapered fiber waveguide coupled with a microspherical cavity. (B) The transmission spectrum of the fiber taper with the microsphere at different positions along the taper. Figures reproduced with permission from Ref. [48], Copyright 2005 AIP.

3.2 Theoretical analysis of all-optical EIT in a single microcavity

In this section, we theoretically analyze the physics of the EIT/Fano resonance in a single cavity. The first case introduced in Figure 8A–D in the previous section includes two different optical modes in the same cavity coupled to a waveguide mode. While the second case, introduced in Figure 9, is slightly different, which includes a single cavity mode and two different waveguide modes, the essential physics of the Fano resonance is the same. In this section, we introduce the theoretical model to explain the physics of EIT/Fano resonance in a single cavity, for the first case.

The taper-cavity coupling system is schematically illustrated in Figure 10A, in which a_1 and a_2 denote the high-Q and the low-Q mode, respectively. The polarizations of the two modes are slightly different, as WGMs are quasi-TE/TM modes and usually they are not exactly parallel or perpendicular to each other [86]. γ_1 (γ_2) and κ_1 (κ_2) represent the intrinsic damping rate and the coupling rate of the high-Q (low-Q) mode, respectively. The waveguide mode c, with an angle θ with a_1, can be decomposed into two orthogonal modes c_1 and c_2, with c_1 being parallel to the polarization of a_1, and a_2 has an angle φ with a_1, as shown in Figure 10B. The Hamiltonian describing this coupling system can be expressed as

$$\begin{aligned} H = & \sum_{j=1,2} \omega_j a_j^{\dagger} a_j + \sum_{k=1,2} \int_{-\infty}^{+\infty} \omega c_k^{\dagger}(\omega) c_k(\omega) d\omega \\ & + i\int_{-\infty}^{+\infty} d\omega \kappa_1(\omega)[c_1^{\dagger}(\omega) a_1 - a_1^{\dagger} c_1(\omega)] \\ & + i\int_{-\infty}^{+\infty} d\omega \kappa_2^h(\omega)[c_1^{\dagger}(\omega) a_2 - a_2^{\dagger} c_1(\omega)] \\ & + i\int_{-\infty}^{+\infty} d\omega \kappa_2^v(\omega)[c_2^{\dagger}(\omega) a_2 - a_2^{\dagger} c_2(\omega)], \end{aligned} \tag{9}$$

where the first two terms represent the free Hamiltonian of the cavity modes (a_1 and a_2) and the waveguide mode (containing two orthogonal modes c_1 and c_2), respectively, and the last three terms describe the coupling between the waveguide mode and the cavity modes with $\kappa_j(\omega)$ ($j=1$, 2h, 2v) as the coupling constant. As the coupling region is small, we have assumed that $\kappa_2^h / \kappa_2^v = \cot^2(\varphi)$.

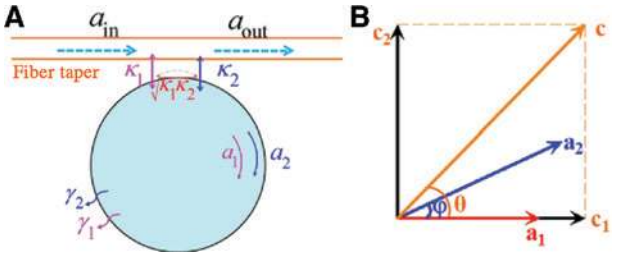

Figure 10: (A) Schematic illustration of the fiber coupled two WGMs system. (B) The polarizations of the two WGMs (a_1 and a_2) and the incident light c (decomposed into two orthogonal waveguide modes c_1 and c_2). Figures reproduced with permission from Ref. [46], Copyright 2011 AIP.

The equations of motion for the waveguide and the cavity modes are as follows:

$$\begin{aligned}
\dot{c}_1(\omega) &= -i\omega c_1(\omega) + \kappa_1(\omega)a_1 + \kappa_2^h(\omega)a_2,\\
\dot{c}_2(\omega) &= -i\omega c_2(\omega) + \kappa_2^v(\omega)a_2,\\
\dot{a}_1 &= \left(-i\omega_1 - \frac{\gamma_1}{2}\right)a_1 - \int_{-\infty}^{+\infty} d\omega\kappa_1(\omega)c_1(\omega),\\
\dot{a}_2 &= \left(-i\omega_2 - \frac{\gamma_2}{2}\right)a_2 - \int_{-\infty}^{+\infty} d\omega\kappa_2^h(\omega)c_1(\omega)\\
&\quad - \int_{-\infty}^{+\infty} d\omega\kappa_2^v(\omega)c_2(\omega).
\end{aligned} \tag{10}$$

Here we have assumed that $\kappa_j(\omega) = \sqrt{\kappa_j/2\pi}$, under the first Markov approximation [87], and the intrinsic loss of the cavities have been taken into account. Solving these coupled-mode equations, we can obtain the time-evolution equations for the cavity modes:

$$\begin{aligned}
\dot{a}_1 &= \left(-i\omega_1 - \frac{\gamma_1}{2} - \frac{\kappa_1}{2}\right)a_1 - \frac{\sqrt{\kappa_1\kappa_2^h}}{2}a_2 - \sqrt{\kappa_1}c_{1\text{in}},\\
\dot{a}_2 &= \left(-i\omega_2 - \frac{\gamma_2}{2} - \frac{\kappa_2^h + \kappa_2^v}{2}\right)a_2 - \frac{\sqrt{\kappa_1\kappa_2^h}}{2}a_1\\
&\quad - \left(\sqrt{\kappa_2^h}c_{1\text{in}} + \sqrt{\kappa_2^v}c_{2\text{in}}\right).
\end{aligned} \tag{11}$$

Using the standard input-output relation $a_{\text{out}}^h = c_{\text{in}}\cos\theta + \sqrt{\kappa_1}a_1 + \sqrt{\kappa_2^h}a_2$, $a_{out}^v = c_{\text{in}}\sin\theta + \sqrt{\kappa_2^v}a_2$ and $|a_{\text{out}}|^2 = |a_{\text{out}}^h|^2 + |a_{\text{out}}^v|^2$, we can calculate the transmission spectrum of this coupling system, where a_{out}^h, a_{out}^v, and a_{out} are the horizontal component of the output field, the vertical component of the output field, and the net output field, respectively.

In a bare cavity, different WGMs are orthogonal and have no direct interaction. However, these two modes can interact indirectly through the taper. From Eq. (11), we find that the taper waveguide does induce an indirect coupling between the two WGMs, with the strength of $\sqrt{\kappa_1\kappa_2^h}$. The interference between the two optical pathways associated with the two modes simultaneously excited in the resonator produces the EIT/Fano resonance. The different transmission lineshapes are mainly determined by γ_j, κ_j and ω_j ($j = 1, 2$). From both experimental and theoretical results, we can see that when both the high-Q and low-Q modes are over-coupled, the transmission spectrum exhibits a Fano lineshape (as shown in the upper first plot in Figure 8C, as an example), while when the high-Q mode is over-coupled and the low-Q mode is under-coupled or critical-coupled, EIT lineshape forms (as shown in the middle and bottom plots in Figure 8C). Also the polarization of the input waveguide mode *c* changes the coupling $\sqrt{\kappa_1\kappa_2^h}$ between the two optical cavity modes, as κ_2^h will change when the incidence polarization is rotated.

Except for the taper-cavity coupling strength and the polarization of the incident light, the frequency detuning of these two modes also affects the output field. For simplicity, we consider the case that the two cavity modes and the incident light all have the same polarization. When the detuning is much larger than the linewidth of the low-Q mode ($\Delta\omega \gg \gamma_2 + \kappa_2$), they have no interaction, and there are two separate dips in the transmission spectrum. When the detuning is smaller than the linewidth of the low-Q mode ($\Delta\omega < \gamma_2 + \kappa_2$), these two modes begin to interact with each other, and the Fano lineshape forms. With further decrease of the frequency detuning, the interaction between the two modes becomes stronger, and the Fano lineshape has larger on/off contrast, as shown in the upper first three plots in Figure 11A. However, when the detuning decreases to zero, the Fano lineshape converts into an EIT lineshape, as shown in the bottom plot in Figure 11A. This can be understood by looking at the phase difference of these two modes ($\arg(a_1) - \arg(a_2)$), shown in Figure 11B, with the four plots corresponding to the conditions in the four plots in Figure 11A, respectively. As shown in the upper first three plots in Figure 11B, when $\omega < \omega_1$, the phase difference is around zero, so the transmission is nearly the summation of these two transmission fields. While for $\omega > \omega_1$, the phase difference is approximately π, so the transmission becomes the subtraction of the two transmission fields. Therefore, at the high-Q mode resonant frequency, it exhibits a peak on the left and a dip on the right (an asymmetric Fano lineshape). When the detuning decreases to zero, it becomes a different case. As shown in the last panel in Figure 11B, before and after the resonant frequency of the high-Q mode, the phase differences are $-\pi/2$ and $\pi/2$, respectively. Therefore, the transmission lineshape is symmetric bilaterally about the high-Q mode resonant frequency. Moreover, as the low-Q mode has a very wide absorption resonant region, it allows the two cavity modes to have a relatively large detuning.

4 Optomechanically induced transparency

Analogously, optomechanically induced transparency (OMIT) is a phenomenon that occurs in cavity optomechanical systems. Cavity optomechanics is an emerging field exploring the interaction between light and mechanical motion in a cavity, which has found broad applications in testing macroscopic quantum physics, high-precision measurements, and quantum information

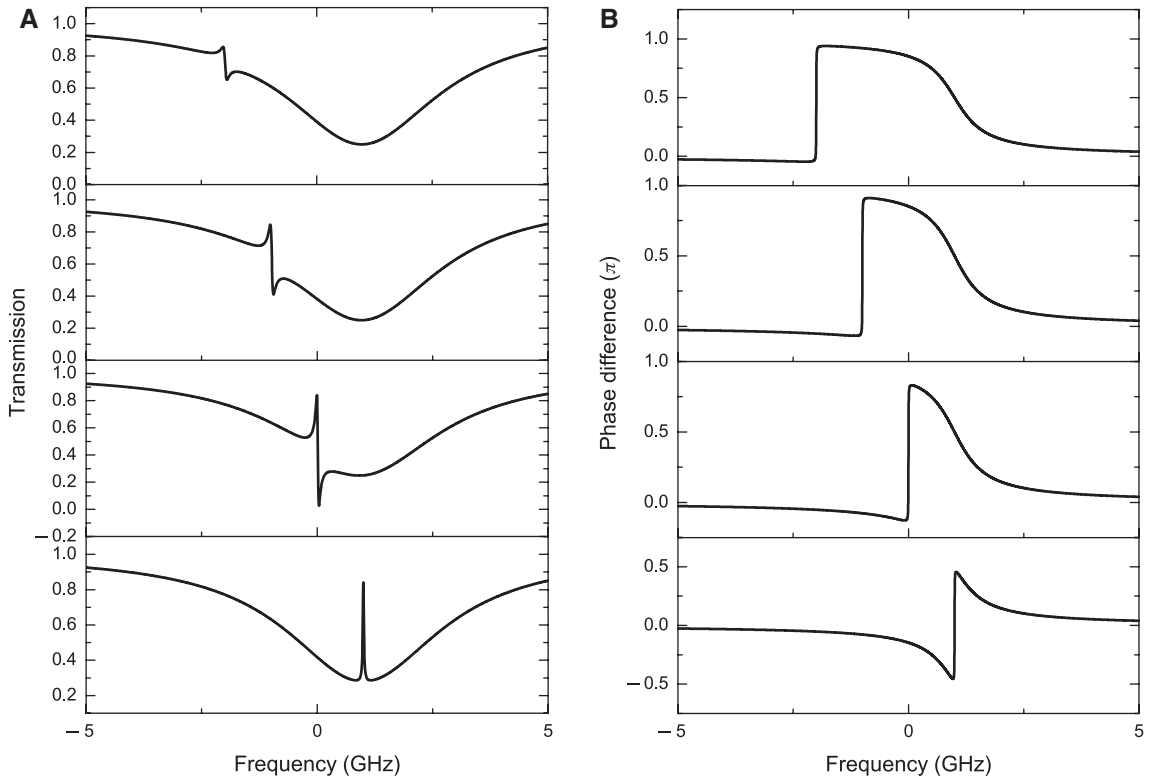

Figure 11: (A) Different transmission spectra with different frequency detunings between the two cavity modes: $\omega_{21}/2\pi = [3, 2, 1, 0]$ GHz. Other parameters are $[\gamma_1, \gamma_2, \kappa_1, \kappa_2]/2\pi = [0.005, 1, 0.1, 3]$ GHz. (B) The relative phase shift of the two cavity modes corresponding to the conditions in the four plots in (A), respectively. Figures reproduced with permission from Ref. [46], Copyright 2011 AIP.

processing [88–93]. The optomechanical interaction originates from the mechanical effect of light, i.e. optical force, which includes two major categories: radiation pressure force (or scattering force) and optical gradient force (or dipole force). Various experimental systems existing such interactions are proposed and investigated, including FP cavities [94, 95], whispering-gallery microcavities [96–99], microring cavities [100], photonic crystal cavities [101–104], membranes [105–108], nanostrings [109], nanorods [110–112], hybrid plasmonic structures [113], optically levitated particles [114–120], cold atoms [121–123], and superconducting circuits [124]. The phenomenon of OMIT was theoretically predicted by Agarwal and Huang [125] and further analyzed for optical pulse storage [126]. It was experimentally observed in a microtoroid system [127], a photonic crystal system [128], a superconducting circuit cavity optomechanical system [129], and a membrane-in-the-middle system [130].

The sketch of a generic cavity optomechanical system is plotted in Figure 12. It shows a Fabry-Pérot cavity consisting of a fixed mirror and a movable mirror mounted on a spring. Because of the radiation pressure force, the optical cavity mode couples to the mechanical oscillation mode of the movable mirror. Using a strong driving field (control field) and a weak probe field, the system can be described by the Hamiltonian

$$H = \omega_c a^\dagger a + \omega_m b^\dagger b + g a^\dagger a (b^\dagger + b) + (\Omega_d^* e^{i\omega_d t} a + \Omega_p^* e^{i\omega_p t} a + H.c.). \quad (12)$$

Here a ($a^\dagger$) is the bosonic annihilation (creation) operator of the optical cavity mode, b ($b^\dagger$) is the bosonic annihilation (creation) operator of the mechanical mode, and ω_c (ω_m) is the corresponding angular resonance frequency. The commutation relations are $[a, a^\dagger] = 1$ and $[b, b^\dagger] = 1$. The displacement operator of the mechanical oscillator is then given by $x = x_{ZPF}(b^\dagger + b)$, where $x_{ZPF} = \sqrt{\hbar/(2m_{eff}\omega_m)}$ is the zero-point fluctuation, with m_{eff} being the effective mass of the mechanical oscillator. The interaction Hamiltonian $H_{int} = g a^\dagger a (b^\dagger + b)$ describes the optomechanical interaction between the optical mode and the mechanical mode, with $g = [\partial\omega_c(x)/\partial x]_{ZPF}$ being the single-photon optomechanical coupling strength. It can be understand by simply considering that the cavity resonance frequency is modulated by the mechanical amplitude and using Taylor expansion, i.e. $\omega_c(x) = \omega_c + x\partial\omega_c(x)/\partial x + \mathcal{O}(x) \simeq \omega_c + g(b^\dagger + b)$. This is in accordance with the result obtained by more rigorous and detailed derivation [131]. Here Ω_c and Ω_p represent the

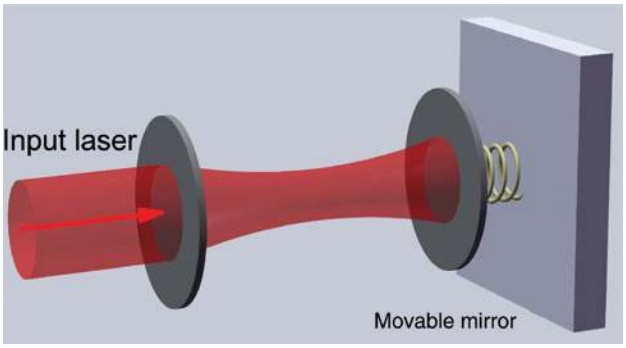

Figure 12: Sketch of a generic cavity optomechanical system. The left mirror is fixed and the right mirror is movable.

control and probe field strengths, ω_c and ω_p are the corresponding laser frequencies. The probe field is assumed to be much weaker than the control field, i.e. $\Omega_p \ll \Omega_d$, so that the probe field does not affect the system dynamics.

First, let us calculate the steady-state response in the frame rotating at the driving laser frequency ω_d, with the absence of the probe field. The equations are given by

$$\begin{aligned} 0 &= \left(i\Delta' - \frac{\kappa}{2}\right)\alpha - i\Omega_d, \\ 0 &= \left(-i\omega_m - \frac{\gamma}{2}\right)\beta - ig|\alpha|^2, \end{aligned} \tag{13}$$

where α and β are the steady-state values of a and b, $\Delta = \omega_d - \omega_c$ is the drive-cavity detuning, $\Delta' = \Delta - g(\beta + \beta^*)$ is the optomechanical-coupling modified detuning, κ is the cavity dissipation rate, and γ is the mechanical dissipation rate.

Next we consider the response after introducing the probe field. As the probe field is weak, the additional response is small. We use the decomposition $a \to \alpha + a_1$ and $b \to \beta + b_1$, where a_1 and b_1 are small compared with α and β, respectively. By applying linearization, it yields the following equations:

$$\begin{aligned} \dot{a}_1 &= \left(i\Delta' - \frac{\kappa}{2}\right)a_1 - iG(b_1 + b_1^*) - i\Omega_p e^{-i(\omega_p - \omega_d)t}, \\ \dot{b}_1 &= \left(-i\omega_m - \frac{\gamma}{2}\right)b_1 - i(G^* a_1 + G a_1^*), \end{aligned} \tag{14}$$

where $G = g\alpha$ is the coherent intracavity field enhanced optomechanical coupling strength. Note that here, a_1 and b_1 are classical mean values.

From Eqs. (5) and (14), we can see that this is similar to the coupled-cavity case, except that the counter-rotating-wave terms appear. In the resolve sideband limit $\omega_m \gg \kappa$, the counter-rotating-wave terms can be neglected. In the frame rotating at the probe laser frequency ω_p, we obtain

$$a_1 = \frac{i\Omega_p}{i(\Delta_p + \Delta') - \frac{\kappa}{2} + \frac{|G|^2}{i(\Delta_p - \omega_m) - \frac{\gamma}{2}}}. \tag{15}$$

It is clear that the intracavity field has the same form as shown in Eq. (6). In this case, the control field plays the role of the coupling between the two cavity modes, and the mechanical mode plays the role of the second cavity mode.

Except for the double-pathway interference interpretation, the physical origin of OMIT can also be understood as follows. The beat of the probe field and the control field induces a time-varying radiation-pressure force with beat frequency Δ_p. Then the mechanical resonator is driven resonantly when the beat frequency matches the mechanical resonance frequency, i.e. $\Delta_p = \omega_m$. Subsequently, the mechanical oscillation leads to the creation of sidebands of the optical field. Considering strong control field and resolved sideband limit, the dominate sideband has the same frequency as the probe field (Figure 13). These processes are coherent, leading to interferences between the sideband and the probe field. Such destructive interference leads to the cancelation of the intracavity field, resulting in a transparency window in the transmission.

In Ref. [127], OMIT is demonstrated in a microtoroidal cavity optomechanical system (Figure 14A). The system supports a mechanical mode with resonance frequency of 51.8 MHz and decay rate of 41 kHz, and the optical decay rate is 15 MHz, which satisfies the resolved sideband condition. A Ti:sapphire control laser with frequency ω_l is modulated at frequency Ω using a broadband phase modulator, which creates two sidebands at $\omega_l \pm \Omega$. By keeping the control laser detuned to the lower motional sideband of the cavity, i.e. $\omega_l - \omega_c = -\omega_m$, the upper sideband at $\omega_l + \Omega$ acts as the probe field, while the lower sideband at $\omega_l - \Omega$ can be neglected in the resolved sideband

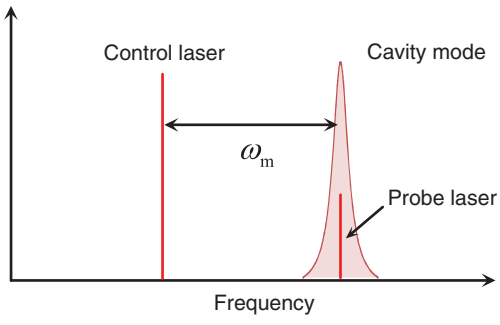

Figure 13: Frequency domain illustration of the control laser, probe laser, and the cavity mode.

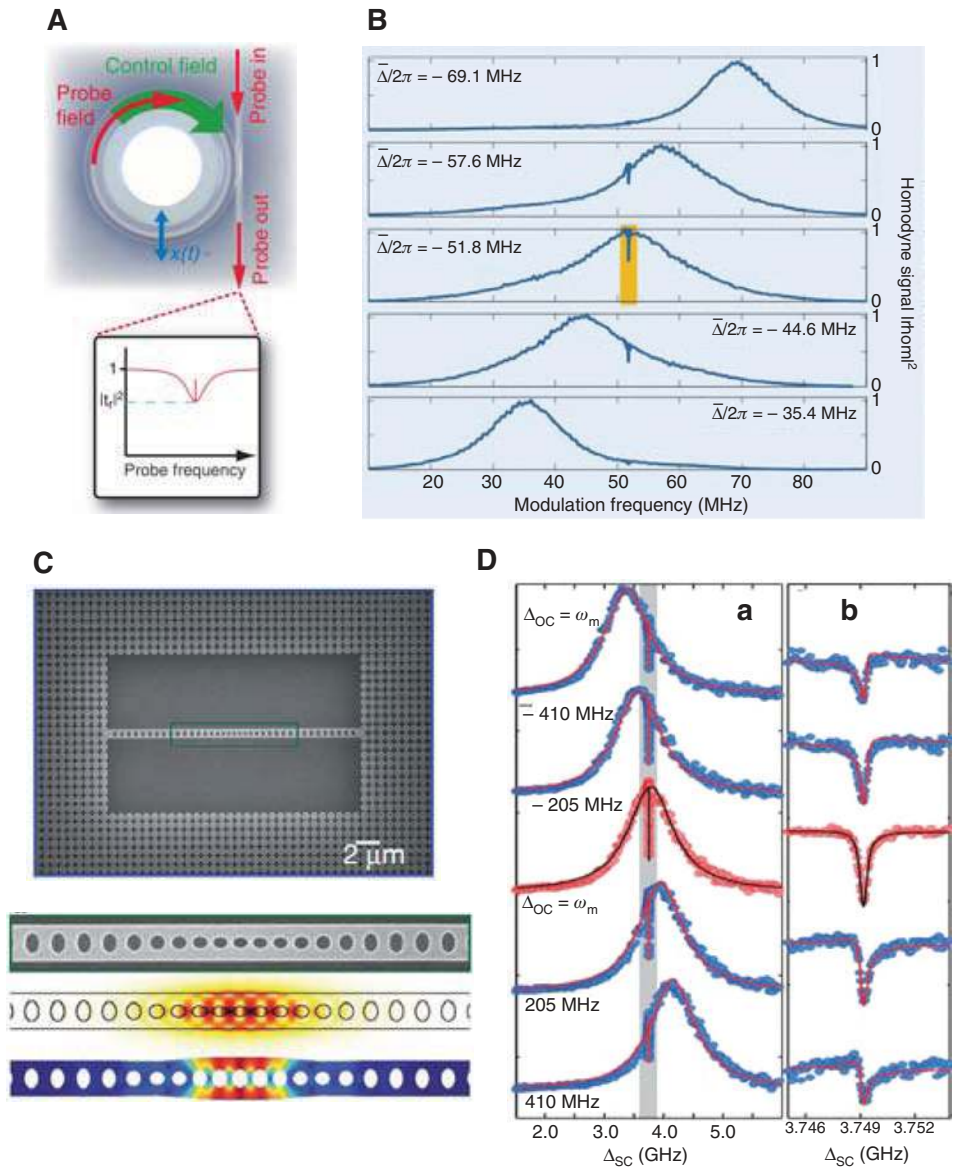

Figure 14: Experimental demonstration of OMIT in WGM microtoroid and photonic crystal nanobeam cavity optomechanical systems. (A) Sketch of the microtoroid system and the transmission. (B) Experimentally observed normalized homodyne traces when the probe frequency is scanned by sweeping the phase modulator frequency for different values of control beam detuning. (C) Scanning electron micrographs of the photonic crystal nanobeam cavity device and the simulation results for the optical and mechanical modes. (D) Measured normalized reflection of the probe beam as a function of the two-photon detuning. Figures reproduced with permission from (A and B) Ref. [127], Copyright 2011 AAAS; (C and D) Ref. [128], Copyright 2011 NPG.

regime. A sweep of the modulation frequency Ω scans the probe field through the cavity resonance, and the transmission properties are shown in Figure 14B. The OMIT window is apparent in the intracavity probe power, and the excitation of the intracavity probe field is suppressed. By varying the control laser detunings, OMIT window still occurs, as long as the two-photon resonance condition is met. Increasing the power of the control field leads to the increase of the depth and width of the OMIT dips. The experiments show that the width of the OMIT dips and the peak value of transmission agree with the theoretical predictions.

In Ref. [128], OMIT is demonstrated in a photonic crystal nanobeam cavity optomechanical system (Figure 14C). The optical wavelength is in the telecommunications band (1550 nm), the single-photon optomechanical coupling rate is 800 kHz, the resonance frequency of the mechanical mode is 3.75 GHz, and the intrinsic optical decay rate is 290 MHz, which is in the resolved sideband regime. The mechanical intrinsic damping rate of 250 kHz

at temperature $T = 8.7$ K, corresponding to a mechanical Q-factor of 1.5×10^4. As shown in Figure 14D, the reflection spectra of the signal beam exhibit EIT lineshape with sharp and tunable dips.

In Ref. [129], OMIT is demonstrated in a superconducting circuit cavity optomechanical system in the microwave region (Figure 15A). The microwave cavity resonance frequency is 7.5 GHz, the cavity decay rate is 170 kHz, the mechanical resonance frequency is 10.69 MHz, and the mechanical decay rate is 30 Hz, corresponding to a mechanical Q factor of 3.6×10^5. The microwave cavity transmission is shown in Figure 15B. As the drive strength increases, the EIT windows appears. In the experiments, it is able to drive the cavity strongly, finally leading to the normal mode splitting.

In a membrane-in-the-middle cavity optomechanical system, OMIT is demonstrated at room temperature [130] (Figure 15C). The input laser operates at a wavelength of 1064 nm, the empty cavity finesse is 6×10^4, and the fundamental membrane vibrational mode has a resonance frequency of 355.6 kHz and a quality factor of 1.22×10^5. In the experiment, the intensity and the phase shift of the beat signal between the transmitted pump and probe fields are measured (Figure 15D), which reflects the transparency window created by the interference.

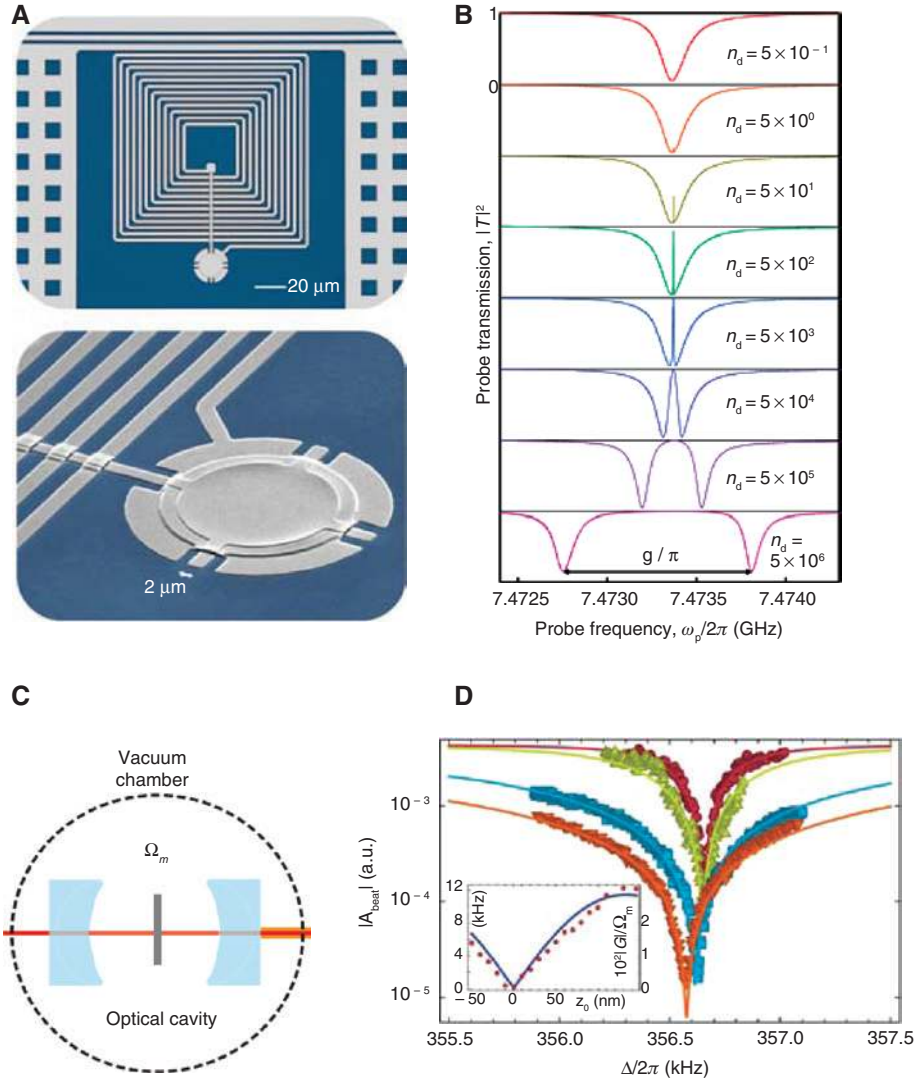

Figure 15: Experimental demonstration of OMIT in superconducting circuit and membrane-in-the-middle cavity optomechanical systems. (A) Micrograph of the microwave resonator formed by a spiral inductor shunted by a parallel-plate capacitor. (B) Normalized microwave cavity transmission in the presence of a drive microwave field, with successive plots for increasing drive amplitude. (C) Schematic description of the membrane-in-the-middle setup. (D) Modulus of the beat between the transmitted pump and probe beams versus the pump-probe detuning for different membrane shifts z_0 with respect to a cavity node. The inset shows the width of the EIT window versus the membrane position z_0. Figures reproduced with permission from (A and B) Ref. [129], Copyright 2011 NPG; (C and D) Ref. [130], Copyright 2013 APS.

For OMIT, If the control field is on resonance with the upper sideband, i.e. $\Delta' = \omega_m$, then the optical signal in the probe beam is amplified [128, 132–134]. This effect is referred to as electromagnetically induced absorption (EIA) [135]. In this case, the interference is constructive instead of destructive. Taking the nonlinear effects into consideration, higher order sidebands will also appear in the transmission spectrum [136–140].

Another kind of induced transparency in cavity optomechanical systems involves one optical mode and two mechanical modes. In Ref. [141], Lin et al. demonstrate the so-called optically induced mechanical transparency in a double-microdisk WGM cavity (Figure 16A) and a zipper nanobeam photonic crystal cavity (Figure 16B). This originates from the internal mechanical coupling between two mechanical modes, as sketched in Figure 16C. One of the mechanical mode is broadband (lossy) flapping mode, while the other mechanical mode is long-lived breathing mode, which is similar to the coupled-cavity case in the all optical domain (Figure 16D). Therefore, the mechanical motion of the lossy flapping mode is excited along two different pathways, either directly into the lossy flapping mode or indirectly through the lossy flapping mode, into the long-lived breathing mode, and then back again into the lossy flapping mode. The two excitation pathways interfere with each other, leading to the EIT-type spectral response. In Ref. [142], Massel et al. investigate a multimode circuit cavity optomechanical system having three degrees of freedom, consisting of a microwave cavity and two micromechanical beams with closely spaced frequencies and no direct interaction (Figure 16E). Similar OMIT spectra can be observed in such a three-mode system (Figure 16F).

More recently, the study of OMIT has attracted much attentions. Huang and Agarwal [143] studied OMIT when the probe field is a squeezed field instead of the ordinary coherent field. They also studied OMIT in a quadratically coupled optomechanical systems where two-phonon processes occur [144]. Dong et al. studied the transient phenomenon of OMIT [145] and OMIT with Bogoliubov mechanical modes [146]. Dong et al. [147] and Kim et al. [148] experimentally demonstrated the Brillouin-scattering-induced transparency and non-reciprocal light storage. Ma et al. [149] studied OMIT in the mechanical-mode splitting regime. Yan et al. [150] investigated the amplification and transparency phenomena in a double-cavity optomechanical system. Jing et al. [151] studied OMIT in a parity-time symmetric microcavity with a tunable gain-to-loss ratio. Schemes for ground-state cooling of mechanical resonators using the EIT interference have also been proposed [152–157].

5 Applications

The EIT effect in optical microcavities has found applications in various fields. The most prominent application is light delay and storage, where light is slowed down or even stopped. Moreover, compared with a single resonance mode, the EIT lineshapes have more sharp peaks, which are desirable in sensing applications. In addition, EIT enables the enhancement of optical field and thus is promising for enhanced light-matter interaction, e.g. optical force enhancement. In this section, we will briefly introduce these applications.

5.1 Light delay and storage

The abnormal dispersion accompanied with the transparency window leads to a reduction of the light group velocity, creating slow light. This is extremely useful for light delays and all-optical buffer. Particularly, when the group velocity is reduced to zero, light is effectively stopped, which can be used to perform optical storage. The light delay and storage have been studied extensively using atomic systems [3–6] after the observation of atomic EIT. Notably, EIT in optical microcavities provides a room-temperature, chip scale, and solid-state platform for realizing light delay and storage. In 2007, Totsuka et al. performed optical pulse propagation experiments in coupled microsphere system and observed a delay of 8.5 ns in the transparency window [36]. In 2011, Safavi-Naeini et al. demonstrated the slow light in a photonic crystal cavity optomechanical system, with a maximum measured transmission delay of 50 ns, corresponding to a group velocity of 40 m/s^2 [128]. Note that increase of the group velocity (fast light) can also be realized by designing an abnormal dispersion region, but in this case, the wave packet distortion should be carefully considered, and one can find that the energy propagation velocity is always less or equal to the velocity of light in vacuum.

One serious limitation of the slow light application is the delay-bandwidth constraint. In principle, traditional EIT system cannot realize large optical delay and large bandwidth simultaneously. The group delay is inversely proportional to the bandwidth within the delay that occurs, thus the delay-bandwidth product is a constant. Much efforts have been done to break this limit. In 2004, Yanik et al. proposed to dynamically modulate the refractive index to generate arbitrarily small group velocity for any light pulse with a given bandwidth. Using coupled cavity arrays [51] or waveguide-coupled cavity system [32], they showed that light pulses can be finally stopped and

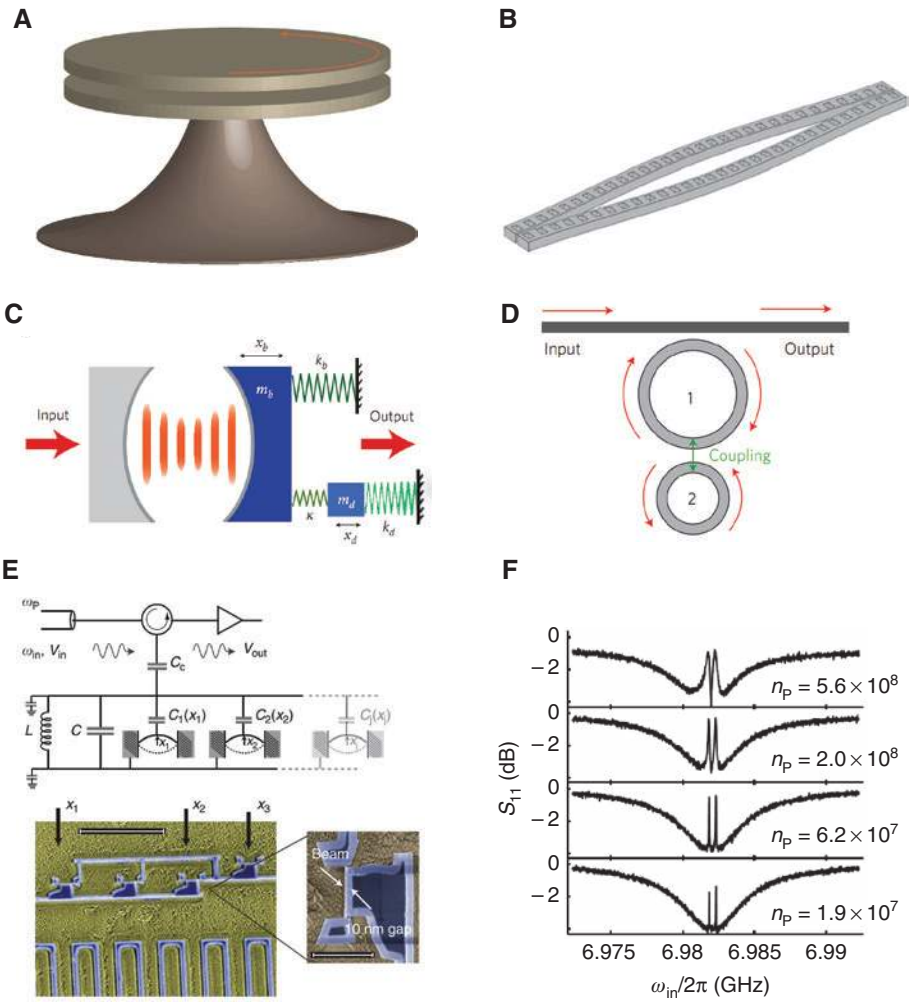

Figure 16: Illustration of the double-disk (A) and zipper nano-optomechanical structures (B). (C) Schematic of an equivalent Fabry-Perot cavity system showing mechanical mode mixing. (D) Photonic analogue to the optomechanical system involving coupled resonators. (E) Schematic description of the microwave-regime multimode cavity optomechanical system. (F) Images of the all-aluminum superconducting sample. Figures reproduced with permission from Ref. [141], Copyright 2010 NPG; Ref. [142], Copyright 2012 NPG.

stored coherently with an all-optical adiabatic and reversible pulse bandwidth compression process (Figure 17A and B). In 2007, Xu et al. [38] reported the demonstration of light storage using fast electro-optical tuning of the resonator refractive index, with storage times longer than the bandwidth-determined photon lifetime of the static device.

5.2 Sensing

The EIT transparency windows typically have much narrower linewidth compared with the background, which is preferred for sensing applications. The narrow linewidth ensures that a small variation of the environment will result in a significant change of the peak position. Therefore, precise sensing can be realized by monitoring the change of the EIT peak. This is particular useful for EIT in plasmonic systems, where the spectrally narrow dark mode cannot directly excited by the plane wave [63]. In 2010, Liu et al. [158] have demonstrated the sensing of the environmental refractive index change using EIT in a planar plasmonic system. Utilizing a cut-out structure on a gold film with a slot dipole antenna supporting bright mode and a slot quadrupole antenna supporting dark mode, they achieved a sensitivity of 588 nm/RIU and a figure of merit of 3.8, which are among the highest values for nanostructure plasmonic sensors (Figure 17C and D). For future applications, the EIT effect is also promising for biosensing applications, for example, measuring the mass concentration of DNA, proteins, and glucose.

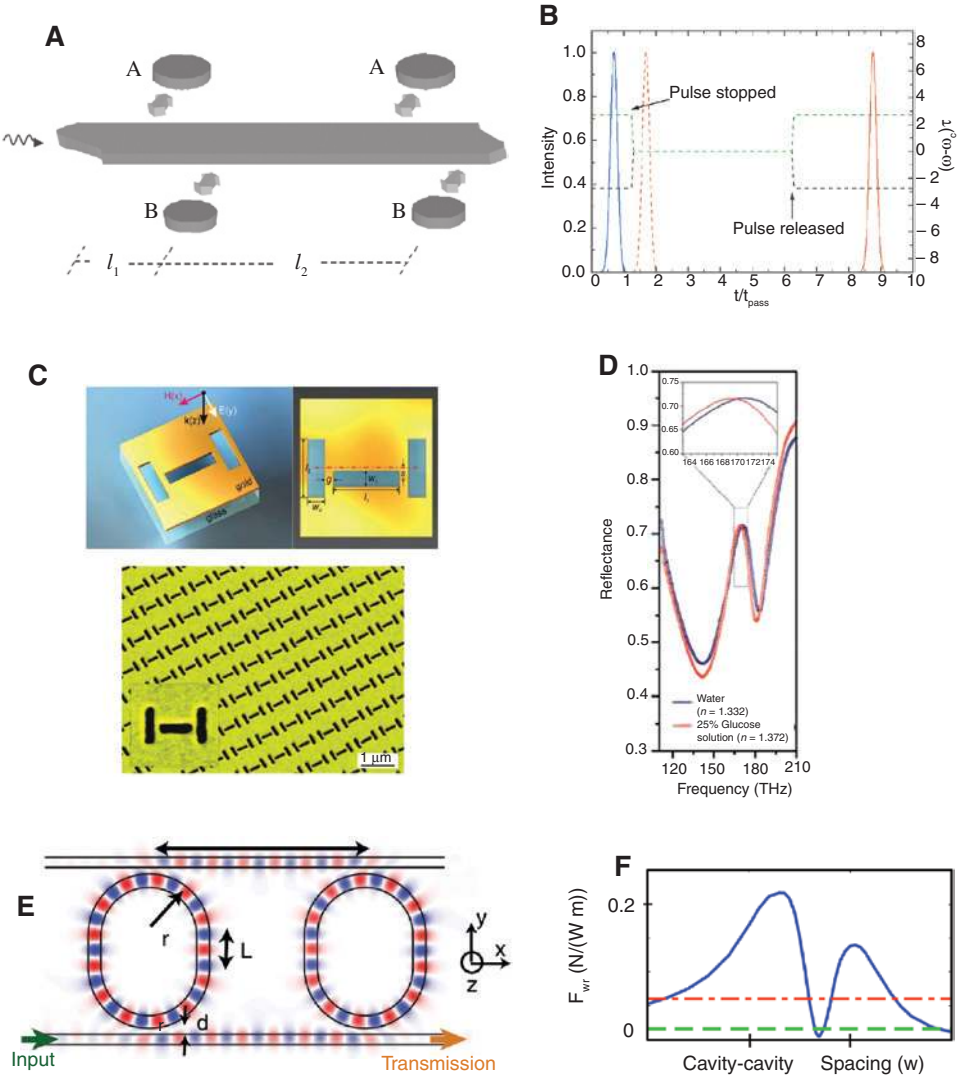

Figure 17: (A) Schematic of a light storage system using a waveguide side coupled to optical cavities. (B) Propagation of an optical pulse through the waveguide-resonator system with the modulation of the cavity resonance frequency. (C) Schematic of the planar metamaterial plasmonic systems that support EIT. (D) Sensing application using the shift of EIT resonance. (E) Diagram of the two-waveguide-two-resonator system that supports EIT. (F) Comparison of the waveguide-resonator pressure between the EIT system and single cavity systems. Figures reproduced with permission from Ref. [32], Copyright 2004 APS; Ref. [158], Copyright 2010 ACS; [159], Copyright 2012 APS.

5.3 Field enhancement

For a waveguide-coupled whispering-gallery mode cavity, the coupling between the waveguide and the cavity has two different roles. On one hand, this coupling guides the input light into the cavity, thus in this sense, strong intracavity field requires a large waveguide-cavity coupling rate. On the other hand, this coupling also results in the dissipation of the light in the cavity, so for this reason, a small waveguide-cavity coupling rate ensures strong intracavity field. Therefore, the waveguide-cavity coupling has a trade-off between coupling light into and out of the cavity, and finally, the intracavity field is limited by this trade-off. The EIT effect can solve this problem by separating these two contradictory roles. In the EIT system, the waveguide-cavity coupling does not strongly affect the linewidth of the EIT transparency window. Near the transparency resonance, the dissipation is small due to destructive interference of the two decaying amplitudes. Therefore, by introducing EIT in the cavity, a large waveguide-cavity coupling rate increases the coupling of light into the cavity but does not increase the coupling of light out of the cavity. This is very useful for field enhancement, which can strongly enhance the light-matter interaction. In 2012, Intaraprasonk and Fan have shown the enhancement of waveguide-cavity optical force [159]. They find

that the EIT effect leads to a drastically enhanced optical force significantly beyond that in conventional waveguide-cavity system without EIT (Figure 17E and F).

6 Summary

In this review article, we mainly focus on EIT in optical microcavity systems, with topics including EIT in coupled cavities, EIT in a single microcavity, and EIT in the cavities involving mechanical motion. We have explained the physics involved in EIT/Fano effect and the quantum interference. The similarities and differences for EIT in different systems are also discussed. Different from the traditional EIT using atomic ensembles, optical microcavities provides a solid-state platform for controlling the light propagation and even enable on-chip manipulation of photons. This provides the most fascinating applications for on-chip optical and quantum information processing like light delay and storage, and it also enables high-sensitivity detection and strong field enhancement. Meanwhile, some critical challenges remain to be solved, e.g. increasing the optical delay, enlarging the bandwidth, breaking the limit of delay-bandwith product, and exploring more applications in enhanced light-matter interaction.

Acknowledgments: This work was supported by the Ministry of Science and Technology of the Peoples Republic of China (MOST) (2013CB328704, 2013CB921904, 2016YFA0301302) and the National Natural Science Foundation of China (NSFC) (11654003, 11474011, 61435001, and 11674390).

References

[1] Harris SE, Field JE, Imamoglu A. Nonlinear optical processes using electromagnetically induced transparency. Phys Rev Lett 1990;64:1107.
[2] Boller KJ, Imamoglu A, Harris SE. Observation of electromagnetically induced transparency. Phys Rev Lett 1991;66:2593.
[3] Kasapi A, Jain M, Yin GY, Harris SE. Electromagnetically induced transparency: propagation dynamics. Phys Rev Lett 1995;74:2447.
[4] Hau LV, Harris SE, Dutton Z, Behroozi CH. Light speed reduction to 17 metres per second in an ultracold atomic gas. Nature 1999;397:594–8.
[5] Phillips DF, Fleischhauer A, Mair A, Walsworth RL, Lukin MD. Storage of light in atomic vapor. Phys Rev Lett 2001;86:783.
[6] Liu C, Dutton Z, Behroozi CH, Hau LV, Observation of coherent optical information storage in an atomic medium using halted light pulses. Nature 2001;409:490–3.
[7] Boyd RW, Gauthier DJ. Controlling the velocity of light pulses. Science 2009;326:1074–7.
[8] Kimble HJ. The quantum internet. Nature 2008;453:1023–30.
[9] Lukin MD, Imamoglu A. Controlling photons using electromagnetically induced transparency. Nature 2001;413:273–6.
[10] Lvovsky AI, Sanders BC, Tittel W. Optical quantum memory. Nat Photonics 2009;3:706–14.
[11] Fleischhauer M, Imamoglu A, Marangos JP. Electromagnetically induced transparency: optics in coherent media. Rev Mod Phys 2005;77:633.
[12] Scully MO. From lasers and masers to phaseonium and phasers. Phys Rep 1992;219:191–201.
[13] Harris SE. Electromagnetically induced transparency. Phys Today 1997;50:37.
[14] Lukin MD, Hemmer P, Scully MO. Resonant nonlinear optics in phase-coherent media. Adv At Mol Opt Phys 2000;42:347–86.
[15] Matsko AB, Kocharovskaya O, Rostovtsev Y, Welch GR, Zibrov AS, Scully MO. Slow, ultraslow, stored, and frozen light. Adv At Mol Opt Phys 2001;46:191–242.
[16] Vitanov, NV, Fleischhauer M, Shore BW, Bergmann K. Coherent manipulation of atoms and molecules by sequential laser pulses. Adv At Mol Opt Phys 2001;46:55–190.
[17] Lukin, MD. Colloquium: trapping and manipulating photon states in atomic ensembles. Rev Mod Phys 2003;75:457.
[18] Arimondo E. Coherent population trapping in laser spectroscopy. Prog Optics 1996;35:259–354.
[19] Marangos JP. Electromagnetically induced transparency. J Mod Opt 1998;45:471–503.
[20] Novikova I, Walsworth RL, Xiao Y. Electromagnetically induced transparency-based slow and stored light in warm atoms. Laser Photonics Rev 201 2;6:333–53.
[21] Fano U. Effects of configuration interaction on intensities and phase shifts. Phys Rev 1961;124:1866.
[22] Imamoglu A, Harris SE. Lasers without inversion: interference of dressed lifetime-broadened states. Opt Lett 1989;14: 1344–6.
[23] Zhang, GZ, Katsuragawa M, Hakuta K, Thompson RI, Stoicheff BP. Sum-frequency generation using strong-field coupling and induced transparency in atomic hydrogen. Phys Rev A 1995;52:1584.
[24] Dalibard J, Castin Y, Molmer K. Wave-function approach to dissipative processes in quantum optics. Phys Rev Lett 1992;68:580.
[25] Gardiner, CW, Parkins AS, Zoller P. Wave-function quantum stochastic differential equations and quantum-jump simulation methods. Phys Rev A 1992;46:4363.
[26] Fan S. Sharp asymmetric line shapes in side-coupled waveguide-cavity systems. Appl Phys Lett 2002;80:908.
[27] Chao CY, Guo LJ. Biochemical sensors based on polymer microrings with sharp asymmetrical resonance. Appl Phys Lett 2003;83:1527.
[28] Liang W, Yang L, Poon JKS, Huang Y, Vahala KJ, Yariv A. Transmission characteristics of a Fabry-Perot etalon-microtoroid resonator coupled system. Opt Lett 2006;31:510–2.
[29] Lu Y, Yao J, Li X, Wang P. Tunable asymmetrical Fano resonance and bistability in a microcavity-resonator-coupled Mach-Zehnder interferometer. Opt Lett 2005;30:3069–71.
[30] Zhou LJ, Poon AW. Fano resonance-based electrically reconfigurable adddrop filters in silicon microring resonator-coupled MachZehnder interferometers. Opt Lett 2007;32:781–3.

[31] Smith DD, Chang H, Fuller KA, Rosenberger AT, Boyd RW. Coupled-resonator-induced transparency. Phys. Rev. A 2004;69:063804.
[32] Yanik MF, Suh W, Wang Z, Fan S. Stopping light in a waveguide with an all-optical analog of electromagnetically induced transparency. Phys Rev Lett 2004;93:233903.
[33] Chu ST, Little BE, Pan W, Kaneko T, Kokubun Y. Second-order filter response from parallel coupled glass microring resonators. IEEE Photonics Technol Lett 1999;11:1426–8.
[34] Naweed A, Farea G, Shopova SI, Rosenberger AT. Induced transparency and absorption in coupled whispering-gallery microresonators. Phys Rev A 2005;71:043804.
[35] Poon JK, Zhu L, DeRose GA, Yariv A. Transmission and group delay of microring coupled-resonator optical waveguides. Opt Lett 2006;31:456–8.
[36] Totsuka K, Kobayashi N, Tomita M. Slow light in coupled-resonator-induced transparency. Phys Rev Lett 2007;98:213904.
[37] Xu Q, Sandhu S, Povinelli ML, Shakya J, Fan S, Lipson M. Experimental realization of an on-chip all-optical analogue to electromagnetically induced transparency. Phys Rev Lett 2006;96:123901.
[38] Xu Q, Dong P, Lipson M. Breaking the delay-bandwidth limit in a photonic structure. Nature Phys 2007;3:406–10.
[39] Xiao YF, Gaddam V, Yang L. Coupled optical microcavities: an enhanced refractometric sensing configuration. Opt Express 2008;16:12538–43.
[40] Xiao Y-F, Min B, Jiang X, Dong C-H, Yang L. Coupling whispering-gallery-mode microcavities with modal coupling mechanism. IEEE J Quant Electon 2008;44:1065–70.
[41] Xiao Y-F, Li M, Liu Y-C, Li Y, Sun X, Gong Q. Asymmetric Fano resonance analysis in indirectly coupled microresonators. Phys Rev A 2010;82:065804.
[42] Li B-B, Xiao Y-F, Zou C-L, et al. Experimental controlling of Fano resonance in indirectly coupled whispering-gallery microresonators. Appl Phys Lett 2012;100:021108.
[43] Xiao YF, Zou XB, Jiang W, Chen YL, Guo GC. Analog to multiple electromagnetically induced transparency in all-optical drop-filter systems. Phys Rev A 2007;75:063833.
[44] Xiao YF, He L, Zhu J, Yang L. Electromagnetically induced transparency-like effect in a single polydimethylsiloxane-coated silica microtoroid. Appl Phys Lett 2009;94:231115.
[45] Dong CH, Zou CL, Xiao YF, Cui JM, Han ZF, Guo GC. Modified transmission spectrum induced by two-mode interference in a single silica microsphere. J Phys B 2009;42:215401.
[46] Li B-B, Xiao Y-F, Zou C-L, et al. Experimental observation of Fano resonance in a single whispering-gallery microresonator. Appl Phys Lett 2011;98:021116.
[47] Yang Y, Saurabh S, Ward J, Chormaic SN. Coupled-mode-induced transparency in aerostatically tuned microbubble whispering-gallery resonators. Opt Lett 2015;40:1834–7.
[48] Chiba A, Fujiwara H, Hotta JI, Takeuchi S, Sasaki K. Fano resonance in a multimode tapered fiber coupled with a microspherical cavity. Appl Phys Lett 2005;86:261106.
[49] Fan S, Joannopoulos JD. Analysis of guided resonances in photonic crystal slabs. Phys Rev B 2002;65:235112.
[50] Yang X, Yu M, Kwong DL, Wong CW. All-optical analog to electromagnetically induced transparency in multiple coupled photonic crystal cavities. Phys Rev Lett 2009;102:173902.
[51] Yanik MF, Fan S. Stopping light all optically. Phys Rev Lett 2004;92:083901.
[52] Zheng C, Jiang XS, Hua SY, et al. Controllable optical analog to electromagnetically induced transparency in coupled high-Q microtoroid cavities. Opt Express 2012;20:18319.
[53] Lin T, Chau FS, Deng J, Zhou GY. Dynamic control of the asymmetric Fano resonance in side-coupled FabryPerot and photonic crystal nanobeam cavities. Appl Phys Lett 2015;107:223105.
[54] Shi P, Zhou GY, Deng J, Tian F, Chau FS. Tuning all-optical analog to electromagnetically induced transparency in nanobeam cavities using nanoelectromechanical system. Sci Rep 2015;5:14379.
[55] Zheng Y, Yang J, Shen Z, et al. Optically induced transparency in a micro-cavity. Light Sci Appl 2015;5:e16072.
[56] Shen Z, Zhang YL, Chen Y, et al. Experimental realization of optomechanically induced non-reciprocity. Nat Photonics 2016;10:657–61.
[57] Ruesink F, Miri, MA, Alù A, Verhagen E. Nonreciprocity and magnetic-free isolation based on optomechanical interactions. Nat Commun 2016;7:13662.
[58] Li J, Yu R, Wu Y. Actively tunable double-Fano and Ramsey-Fano resonances in photonic molecules and improved sensing performance. Phys Rev A 2016;94:063822.
[59] Tassin P, Zhang L, Zhao R, Jain A, Koschny T, Soukoulis CM. Electromagnetically induced transparency and absorption in metamaterials: the radiating two-oscillator model and its experimental confirmation. Phys Rev Lett 2012;109:187401.
[60] Miroshnichenko AE, Flach S, Kivshar YS. Fano resonances in nanoscale structures. Rev Mod Phys 2010;82:2257.
[61] Hao F, Sonnefraud Y, Dorpe PV, Maier SA, Halas NJ, Nordlander P. Symmetry breaking in plasmonic nanocavities: subradiant LSPR sensing and a tunable Fano resonance. Nano Lett 2008;8:3983–8.
[62] Luk'yanchuk B, Zheludev NI, Maier SA, Halas NJ, Nordlander P. The Fano resonance in plasmonic nanostructures and metamaterials. Nat Mater 2010;9:707–15.
[63] Zhang S, Genov DA, Wang Y, Liu M, Zhang X. Plasmon-induced transparency in metamaterials. Phys Rev Lett 2008;101:047401.
[64] Papasimakis N, Fedotov VA, Zheludev NI, Prosvirnin SL. Metamaterial analog of electromagnetically induced transparency. Phys Rev Lett 2008;101:253903.
[65] Tassin P, Zhang L, Koschny T, Economou EN, Soukoulis CM. Low-loss metamaterials based on classical electromagnetically induced transparency. Phys Rev Lett 2009;102:053901.
[66] Chiam SY, Singh R, Rockstuhl C, Lederer F, Zhang W, Bettiol AA. Analogue of electromagnetically induced transparency in a terahertz metamaterial. Phys Rev B 2009;80:153103.
[67] Rahmani M, Luk'yanchuk B, Hong M. Fano resonance in novel plasmonic nanostructures. Laser Photonics Rev 2013;7:329–49.
[68] Vahala KJ. Optical microcavities. Nature 2003;424:839–46.
[69] Braginsky VB, Gorodetsky ML, Ilchenko VS. Quality-factor and nonlinear properties of optical whispering-gallery modes. Phys Lett A 1989;137:393–7.
[70] Armani DK, Kippenberg TJ, Spillane SM, Vahala KJ. Ultra-high-Q toroid microcavity on a chip. Nature 2003;421:925–8.
[71] Aoki T, Dayan B, Wilcut E, et al. Observation of strong coupling between one atom and a monolithic microresonator. Nature 2006;443: 671–4.
[72] Park YS, Cook AK, Wang H. Cavity QED with diamond nanocrystals and silica microspheres. Nano Lett 2006;6:2075–9.

[73] Ilchenko VS, Savchenkov AA, Matsko AB, Maleki L. Nonlinear optics and crystalline whispering gallery mode cavities. Phys Rev Lett 2004;92:043903.
[74] Sandoghdar V, Treussart F, Hare J, Lefevre-Seguin V, Raimond JM, Haroche S. Very low threshold whispering-gallery-mode microsphere laser. Phys Rev A 1996;54:R1777.
[75] Vollmer F, Braun D, Libchaber A, Khoshsima M, Teraoka I, Arnold S. Protein detection by optical shift of a resonant microcavity. Appl Phys Lett 2002;80:4057.
[76] White IM, Oveys H, Fan X. Liquid-core optical ring-resonator sensors. Opt Lett 2006;31:1319–21.
[77] Armani AM, Kulkarni RP, Fraser SE, Flagan RC, Vahala KJ. Label-free, single-molecule detection with optical microcavities. Science 2007;317:783–7.
[78] Vollmer F, Arnold S, Keng D. Single virus detection from the reactive shift of a whispering-gallery mode. Proc Natl Acad Sci USA 2008;105:20701–4.
[79] Zhu J, Ozdemir SK, Xiao Y-F, et al. On-chip single nanoparticle detection and sizing by mode splitting in an ultrahigh-Q microresonator. Nat Photon 2010;4:46–9.
[80] He L, Ozdemir SK, Zhu J, Kim W Yang L. Detecting single viruses and nanoparticles using whispering gallery microlasers. Nature Nanotech 2011;6:428432.
[81] Li B-B, Clements WR, Yu X-C, Shi K, Gong Q, Xiao Y-F. Single nanoparticle detection using split-mode microcavity Raman lasers. Proc Natl Acad Sci USA 2014;111:1465714662.
[82] Ozdemir SK, Zhu J, Yang X, et al. Highly sensitive detection of nanoparticles with a self-referenced and self-heterodyned whispering-gallery Raman microlaser. Proc Natl Acad Sci USA 2014;111:E3836E3844.
[83] Peng B, Özdemir SK, Chen W, Nori F, Yang L. What is and what is not electromagnetically induced transparency in whispering-gallery microcavities. Nat Commun 2014;5:5082.
[84] Sun HC, Liu YX, Hou I, You JQ, Il'Ichev E, Nori F. Electromagnetically induced transparency and autler-townes splitting in superconducting flux quantum circuits. Phys Rev A 2013;89:063822.
[85] He L, Xiao Y-F, Dong C, Zhu J, Gaddam V, Yang L. Compensation of thermal refraction effect in high-Q toroidal microresonator. Appl Phys Lett 2008;93:201102.
[86] Min B, Yang L, Vahala K. Perturbative analytic theory of an ultrahigh-Q toroidal microcavity. Phys Rev A 2007;76:013823.
[87] Gardiner CW, Zoller P. Quantum noise. 3rd ed. Berlin: Springer, 2004.
[88] Aspelmeyer M, Kippenberg TJ, Marquardt F. Cavity optomechanics. Rev Mod Phys 2014;86:1391.
[89] Meystre P. A short walk through quantum optomechanics. Ann Phys 2013;525:215–33.
[90] Kippenberg TJ, Vahala KJ. Cavity optomechanics: back-action at the mesoscale. Science 2008;321:1172–6.
[91] Hu YW, Xiao YF, Liu YC, Gong QH. Optomechanical sensing with on-chip microcavities. Front Phys 2013;8:475–90.
[92] Liu YC, Hu YW, Wong CW, Xiao YF. Review of cavity optomechanical cooling. Chinese Physics B 2013;22:114213.
[93] Liu YC, Xiao YF. Macroscopic mechanical systems are entering the quantum world. National Science Review 2015;2:9–10.
[94] Gigan S, Böhm HR, Paternostro M, et al. Self-cooling of a micromirror by radiation pressure. Nature 2006;444:67–71.
[95] Arcizet O, Cohadon PF, Briant T, Pinard M, Heidmann A. Radiation-pressure cooling and micromechanical instability of a micromirror. Nature 2006;444:71–5.
[96] Kippenberg TJ, Rokhsari H, Carmon T, Scherer A, Vahala KJ. Radiation-pressure induced parametric instability. Phys Rev Lett 2005;95:033901.
[97] Tomes M, Carmon T. Photonic micro-electromechanical systems vibrating at X-band (11-GHz) rates. Phys Rev Lett 2009;102:113601.
[98] Ma R, Schliesser A, Del'Haye P, Dabirian A, Anetsberger G, Kippenberg TJ. Radiation-pressure-driven vibrational modes in ultrahigh-Q silica microspheres. Opt Lett 2007;32:2200–2.
[99] Jiang X, Lin Q, Rosenberg J, Vahala K, Painter O. High-Q double-disk microcavities for cavity optomechanics. Opt Express 2009;17:20911–9.
[100] Wiederhecker GS, Chen L, Gondarenko A, Lipson M. Controlling photonic structures using optical forces. Nature 2009;462:633–6.
[101] Eichenfield M, Camacho R, Chan J, Vahala KJ, Painter O. A picogram- and nanometre-scale photonic-crystal optomechanical cavity. Nature 2009;459:550–5.
[102] Eichenfield M, Chan J, Camacho RM, Vahala KJ, Painter O. Optomechanical crystals. Nature 2009;462:78–82.
[103] Li Y, Zheng J, Gao J, Shu J, Aras MS, Wong CW. Design of dispersive optomechanical coupling and cooling in ultra-high-Q/V slot-type photonic crystal cavities. Opt Express 2010;18:23844–56.
[104] Zheng J, Li Y, Aras MS, Stein A, Shepard KL, Wong CW. Parametric optomechanical oscillations in two-dimensional slot-type high-Q photonic crystal cavities. App Phys Lett 2012;100:211908.
[105] Thompson JD, Zwickl BM, Jayich AM, Marquardt F, Girvin SM, Harris JGE. Strong dispersive coupling of a high-finesse cavity to a micromechanical membrane. Nature 2008;452:72–5.
[106] Cheung HK, Law CK. Nonadiabatic optomechanical Hamiltonian of a moving dielectric membrane in a cavity. Phys Rev A 2011;84:023812.
[107] Bui CH, Zheng J, Hoch SW, Lee LYT, Harris JGE, Wong CW. High-reflectivity, high-Q micromechanical membranes via guided resonances for enhanced optomechanical coupling. App Phys Lett 2012;100:021110.
[108] Li HK, Liu YC, Yi X, Zou CL, Ren XX, Xiao YF. Proposal for a near-field optomechanical system with enhanced linear and quadratic coupling. Phys Rev A 2012;85:053832.
[109] Anetsberger G, Arcizet O, Unterreithmeier QP, et al. Near-field cavity optomechanics with nanomechanical oscillators. Nat Phys 2009;5:909–14.
[110] Li M, Pernice WHP, Xiong C, Baehr-Jones T, Hochberg M, Tang HX. Harnessing optical forces in integrated photonic circuits. Nature 2008;456:480–4.
[111] Favero I, Stapfner S, Hunger D, et al. Fluctuating nanomechanical system in a high finesse optical microcavity. Opt Express 2009;17:12813–20.
[112] Zheng J, Sun X, Li Y, et al. Femtogram dispersive L3-nanobeam optomechanical cavities: design and experimental comparison. Opt Express 2012;20:26484–98.
[113] Hu YW, Li BB, Liu YC, Xiao YF, Gong QH. Hybrid photonic-plasmonic mode for refractometer and nanoparticle trapping. Opt Commun 2013;291:380–5.
[114] Chang DE, Regal CA, Papp SB, et al. Cavity opto-mechanics using an optically levitated nanosphere. Proc Natl Acad Sci USA 2010;107:1005–10.

[115] Romero-Isart O, Juan ML, Quidant R, Cirac JI. Toward quantum superposition of living organisms. New J Phys 2010;12:033015.
[116] Li T, Kheifets S, Raizen MG. Millikelvin cooling of an optically trapped microsphere in vacuum. Nat Phys 2011;7:527–30.
[117] Gieseler J, Deutsch B, Quidant R, Novotny L. Subkelvin parametric feedback cooling of a laser trapped nanoparticle. Phys Rev Lett 2012;109:103603.
[118] Pender GAT, Barker PF, Marquardt F, Millen J, Monteiro TS. Optomechanical cooling of levitated spheres with doubly resonant fields. Phys Rev A 2012;85:021802(R).
[119] Yin ZQ, Li T, Feng M. Three-dimensional cooling and detection of a nanosphere with a single cavity. Phys Rev A 2011;83:013816.
[120] Yin ZQ, Li T, Zhang X, et al. Large quantum superpositions of a levitated nanodiamond through spin-optomechanical coupling. Phys Rev A 2013;88:033614.
[121] Brennecke F, Ritter S, Donner T, Esslinger T. Cavity optomechanics with a Bose-Einstein condensate. Science 2008;322:235–8.
[122] Murch KW, Moore KL, Gupta S, Stamper-Kurn DM. Observation of quantum-measurement backaction with an ultracold atomic gas. Nat Phys 2008;4:561–4.
[123] Zhang K, Meystre P, Zhang W. Role reversal in a Bose-condensed optomechanical system. Phys Rev Lett 2012;108:240405.
[124] Regal CA, Teufel JD, Lehnert KW. Measuring nanomechanical motion with a microwave cavity interferometer. Nat Phys 2008;4:555–60.
[125] Agarwal GS, Huang S. Electromagnetically induced transparency in mechanical effects of light. Phys Rev A 2010;81:041803(R).
[126] Chang DE, Safavi-Naeini AH, Hafezi M, Painter O. Slowing and stopping light using an optomechanical crystal array. New J Phys 2011;13:023003.
[127] Weis S, Rivière R, Deléglise S, et al. Optomechanically induced transparency. Science 2010;330:1520–3.
[128] Safavi-Naeini AH, Alegre TPM, Chan J, et al. Electromagnetically induced transparency and slow light with optomechanics. Nature 2011;472:69–73.
[129] Teufel JD, Li D, Allman MS, et al. Circuit cavity electromechanics in the strong-coupling regime. Nature 2011;471:204–8.
[130] Karuza M, Biancofiore C, Bawaj M, et al. Optomechanically induced transparency in a membrane-in-the-middle setup at room temperature. Phys Rev A 2013;88:013804.
[131] Law CK. Interaction between a moving mirror and radiation pressure: a Hamiltonian formulation. Phys Rev A 1995;51:2537–41.
[132] Massel F, Heikkilä TT, Pirkkalainen JM, et al. Microwave amplification with nanomechanical resonators. Nature 2011;480:351–4.
[133] Hocke F, Zhou X, Schliesser A, Kippenberg TJ, Huebl H, Gross R. Electromechanically induced absorption in a circuit nanoelectromechanical system. New J Phys 2012;14:123037.
[134] Qu K, Agarwal GS. Phonon-mediated electromagnetically induced absorption in hybrid opto-electromechanical systems. Phys Rev A 2013;87:031802(R).
[135] Lezama A, Barreiro S, Akulshin A, Electromagnetically induced absorption. Phys Rev A 1999;59:4732.
[136] Xiong H, Si LG, Zheng AS, Yang X, Wu Y. Higher-order sidebands in optomechanically induced transparency. Phys Rev A 2012;86:013815.
[137] Lemonde MA, Didier N, Clerk AA. Nonlinear interaction effects in a strongly driven optomechanical cavity. Phys Rev Lett 2013;111:053602.
[138] Børkje K, Nunnenkamp A, Teufel JD, Girvin SM. Signatures of nonlinear cavity optomechanics in the weak coupling regime. Phys Rev Lett 2013;111:053603.
[139] Liu YC, Xiao YF, Chen YL, Yu XC, Gong QH. Parametric down-conversion and polariton pair generation in optomechanical systems. Phys Rev Lett 2013;111:083601.
[140] Kronwald A, Marquardt F. Optomechanically induced transparency in the nonlinear quantum regime. Phys Rev Lett 2013;111:133601.
[141] Lin Q, Rosenberg J, Chang D, et al. Coherent mixing of mechanical excitations in nano-optomechanical structures. Nat Photonics 2010;4:236–42.
[142] Massel F, Cho SU, Pirkkalainen JM, Hakonen PJ, Heikkilä TT, Sillanpää MA. Multimode circuit optomechanics near the quantum limit. Nat Commun 2012;3:987.
[143] Huang S, Agarwal GS. Electromagnetically induced transparency with quantized fields in optocavity mechanics. Phys Rev A 2011;83:043826.
[144] Huang S, Agarwal GS. Electromagnetically induced transparency from two-phonon processes in quadratically coupled membranes. Phys Rev A 2011;83:023823.
[145] Dong CH, Fiore V, Kuzyk MC, Tian L, Wang H. Optical wavelength conversion via optomechanical coupling in a silica resonator. Annalen der Physik 2015;527:100.
[146] Dong CH, Fiore V, Kuzyk MC, Wang H. Transient optomechanically induced transparency in a silica microsphere. Phys Rev A 2013;87:055802.
[147] Dong CH, Shen Z, Zou CL, Zhang YL, Fu W, Guo GC. Brillouin scattering induced transparency and non-reciprocal light storage. Nat Commun 2015;6:6193.
[148] Kim JH, Kuzyk MC, Han K, Wang H, Bahl G. Non-reciprocal Brillouin scattering induced transparency. Nature Physics 2015;11:275–80.
[149] Ma J, Cai Y, Si LG, Xiong H, Yang XX, Wu Y. Optomechanically induced transparency in the mechanical-mode splitting regime. Opt Lett 2014;39:4180–3.
[150] Yan XB, Jia WZ, Li Y, Wu JH. Optomechanically induced amplification and perfect transparency in double-cavity optomechanics. Front Phys 2015;10:351–7.
[151] Jing H, Özdemir SK, Geng Z, et al. Optomechanically-induced transparency in parity-time-symmetric microresonators. Sci Rep 2015;5:9663.
[152] Gu WJ, Li GX. Quantum interference effects on ground-state optomechanical cooling. Phys Rev A 2013;87:025804.
[153] Liu YC, Xiao YF, Luan X, Wong CW. Ground state cooling of mechanical motion through coupled cavity interactions in the unresolved sideband regime. CLEO (Optical Society of America) 2013:p.QM2B.2.
[154] Liu YC, Xiao YF, Luan X, Gong QH, Wong CW. Coupled cavities for motional ground state cooling and strong optomechanical coupling. Phys Rev A 2015;91:033818.
[155] Guo YJ, Li K, Nie WJ, Li Y. Electromagnetically-induced-transparency-like ground-state cooling in a double-cavity optomechanical system. Phys Rev A 2014;90:053841.

[156] Ojanen T, Børkje K. Ground-state cooling of mechanical motion in the unresolved sideband regime by use of optomechanically induced transparency. Phys Rev A 2014;90:013824.
[157] Liu YC, Xiao YF, Luan XS, Gong QH, Wong CW. Optomechanically-induced-transparency cooling of massive mechanical resonators to the quantum ground state. Sci China-Phys Mech Astron 2015;58:050305.
[158] Liu N, Weiss T, Mesch M, et al. Planar metamaterial analogue of electromagnetically induced transparency for plasmonic sensing. Nano Lett 2010;10:1103.
[159] Intaraprasonk V, Fan S. Enhancing the waveguide-resonator optical force with an all-optical on-chip analog of electromagnetically induced transparency. Phys Rev A 2012;86:063833.